6. GRID DESIGN AND ACCURACY IN NUMERICAL SIMULATIONS OF VARIABLY SATURATED FLOW IN RANDOM MEDIA: REVIEW AND NUMERICAL ANALYSIS

6.1 Introduction

Most numerical stochastic models are based either on the Monte Carlo technique or on single large realizations. The numerical stochastic models technically consists of three major parts or modules:

1.) Random fields are generated to represent realizations of the stochastic input variables (random field variables, RFV, see section 2.5.1 and chapter 3) such as the saturated hydraulic conductivity.

2.) Using the random field(s) as input, a standard finite difference or finite element model (or any other numerical technique) is applied to solve the flow equation deterministically i.e., to compute the dependent variables (head and flux) at each location in space and time - the latter only for transient simulations (see chapter 5). Step 1 and 2 may be repeated several times to obtain a sample of realizations that will be large enough to represent the ensemble with only a small statistical error (Monte Carlo simulation). By invoking the ergodicity assumption (chapter 2) a single large simulation is sometimes used by itself to represent the ensemble (Ababou, 1988; Russo, 1991).

3.) The last step of a stochastic simulation will be to employ statistical analysis on the deterministic results i.e., to find, for example, the histogram, mean, variance, and covariance of the resulting random fields of output variables (see e.g. chapter 3.4).

A number of design criteria have to be considered to assure that the Monte Carlo analysis will be accurate when analyzing unsaturated flow in heterogeneous media (numerical stochastic approach). Discretization of the numerical grid and the time stepping have long been recognized

as an important input parameter to assure the accuracy of numerical models for unsaturated flow in homogeneous media (Fletcher, 1988). The grid design of Monte Carlo simulations must in addition assure results that are also accurate in the stochastic sense. The working hypothesis that will be tested in this chapter is that the grid design for Monte Carlo simulations (which are evaluated for their statistical information content) is different from that required for deterministic simulations (which are evaluated for their absolute information content). In this chapter, grid design criteria for the stochastic simulation of unsaturated flow are developed based on the empirical statistical analysis of single large simulations for which the ergodicity assumption can be invoked.

From the perspective of the numerical modeler the deterministic approach is merely a special case of the stochastic approach. As shown above, the deterministic method is embedded in the stochastic approach as one of three major modules. Hence, the list of important design parameters includes several critical elements that are unique to the stochastic approach:

module 1: The simulated random fields have to converge in mean square to the desired moment and statistical distribution specifications. This restricts the choice of the minimum relative correlation length $\boldsymbol{\lambda}' = \boldsymbol{\lambda}/\mathbf{b}$ ($\boldsymbol{\lambda}$: vector of directional correlation lengths; vectors are indicated by lower boldface letters; **b**: vector of the length of a block in each dimension; a block is a discrete, homogeneous unit within the heterogeneous domain). When using SRFFT or TB type random field generators the convergence requirement will in general impose certain limits on the minimum relative size of the random field $\mathbf{d}' = \mathbf{d}/\boldsymbol{\lambda}$ (**d**: length vector of the domain size e.g., depth and width of a vertical 2-D simulation domain). The generated random field should be free of any artificially introduced patterns such as the line-patterns resulting from some versions of the turning bands random field generator (see chapter 3.4)(Gutjahr, 1989; Tompson et al., 1989).

module 2: The general formulation of the finite difference or finite element solution algorithm, the element size $\Delta\mathbf{x}$, and the time-stepping Δt must be chosen to assure stability, consistency, and convergence of the solution. Since the unsaturated flow problem is nonlinear,

special demands are placed on the element size $\Delta\mathbf{x}$ and the dimensionless size of the random blocks $\mathbf{b}/\Delta\mathbf{x}$ in the simulated domain. These criteria are distinctly different from criteria used to model saturated flow, as discussed below. In transient simulations of unsaturated flow, the time-step Δt must also be chosen with care.

module 3: For the stochastic analysis, effects from deterministic boundary conditions, the stationarity and ergodicity of the simulation, and the degree of resolution of the heterogenous field have to be taken into account. The limits imposed by these requirements are often mutually dependent because computing resources are limited. The relative correlation length $\lambda' = \lambda/\mathbf{b}$, for example, is a measure of the resolution of the heterogeneous field: the larger λ', the finer the structure of the random field i.e., more of the true variance of the continuous random field variable will be captured by the simulation. However, the total size of the random field domain must also be large with respect to the correlation length to assure that the spectrally generated random fields accurately represent the desired moments (SRFFT method, chapter 3), to minimize boundary effects, and to meet the requirements of the ergodicity assumption in a single large realization (see chapters 2 and 3). Given a maximum domain size $\mathbf{d}/\Delta\mathbf{x}$ (dictated by the limits of the computer), an optimal compromise choice for the two parameters $\mathbf{d}/\lambda$, $\lambda/\mathbf{b}$, and $\mathbf{b}/\Delta\mathbf{x}$ has to be found.

While stochastic numerical models are increasingly applied to analyze the effects of heterogeneities in the unsaturated zone, there is little guidance in the literature regarding the design of the numerical grid used for such simulations. Commonly, vertical discretization is chosen on the order of a few centimeter, while horizontal discretization maybe on the order of several tens of centimeters. Also, few analytical or empirical results are available for determining a meaningful relative correlation length λ'. The smallest perturbation resolved by any numerical grid has a wavelength twice the element-size (see chapter 3). Thus, the statistical resolution requirement that $\mathbf{b} << \lambda$. The resolution λ' is commonly chosen to be between two and five (e.g. Ababou, 1988; Hopmans, 1989; Russo, 1991).

While such design criteria have been applied to stochastic simulations of unsaturated

flow, most have originally been developed for solving the saturated flow equation. The immediate application of these criteria to also solve Richards equation (4-1) seems not warranted without a closer examination of the difficulties that may arise from the nonlinear character of Richards equation. The purpose of this chapter is to closely examine some of the most important numerical design criteria mentioned. Two-dimensional, heterogeneous, unsaturated steady state flow in a single, large vertical flow domain is simulated i.e., the stationarity and ergodicity assumptions are invoked (see also Ababou, 1988; Russo, 1991). The difficulties encountered in deriving analytical solutions limit closed form stochastic analyses to first or second order approximations (Yeh et al., 1985a,b; Ababou, 1988; this work, chapter 4). This limitation renders most analytical solutions unsuitable for comparison with numerical simulations in highly disordered media. For the same reasons, it is also difficult to develop exact modeling criteria based on a rigorous truncation and error analysis of the nonlinear numerical model.

A common way to empirically establish certain grid design criteria, is to vary the grid parameters and to compare the results among themselves (Hopmans et al., 1988) and possibly with analytical solutions, if these are available. The obvious drawback of the method is that the criteria may only apply to a particular situation. My hope, however, is that the following examples will establish some general guidelines regarding the design of stochastic computer simulations. Numerical experiments are implemented to analyze the sensitivity of stochastic solutions with respect to:

* the absolute length of the grid-elements $\Delta \mathbf{x}$
* the number $\mathbf{b' = b/\Delta x}$ of elements within each homogeneous block
* the size $\lambda' = \lambda/\mathbf{b}$ of each block relative to the correlation length of the stochastic input variables
* the size $\mathbf{d'} = \mathbf{d}/\lambda$ of the simulation domain relative to the correlation length of the stochastic input variables

Known limitations on grid-design are summarized in section 6.2. The details of the simulations

are given in section 6.3. Results are discussed in section 6.4. Analytical solutions developed in chapter 4 will be used to verify the numerical solutions. A comparison with simulations by other authors is made in section 6.5. A summary is given in section 6.6.

6.2 Review of Some Theoretical Considerations Regarding Numerical Accuracy

6.2.1 Grid Size

Well known criteria to assure accurate and stable solutions are only available for determining the maximum element-size and the time-step in some deterministic FD or FE methods (Fletcher, 1988). Ababou (1988) derived a grid discretization or Peclet number based on an error and truncation analysis of the particular finite difference model he developed for the simulation of unsaturated, transient flow. For vertical flow in a soil described by Gardner's model for K(h), the grid Peclet number was found to be:

$$\alpha \Delta x_2 < 2 \qquad \textbf{(6-1)}$$

If this or other similar criteria are strictly applied to the simulation of flow in heterogeneous soils, the largest possible value of α in the random field dictates the discretization in space. Similar arguments can be made for the discretization in time. Since α is commonly on the order of 10^{-3} to 10^{-1} cm^{-1}, vertical discretization in an unsaturated heterogeneous flow model is often chosen to be between 2 cm and 10 cm (Ababou, 1988; Hopmans et al., 1988; Ünlü et al., 1990; Russo, 1991). For horizontal grid lengths Δx_1, Hopmans et al. (1988) found little difference in the stochastic results of two sets of Monte Carlo simulations with Δx_1 = 12.5 cm and Δx_1 = 25 cm, respectively. Other authors chose similar horizontal grid-lengths without further specifying the reasons for their choice. The vertical grid discretization in Hopmans et al. (1988) is determined by reducing Δx_2 systematically until no change is observed in the results.

However, the numerical errors resulting from any particular choice of finite difference or finite element method are only one of a number of possible error sources in the stochastic

simulation. An important limitation arises from the discrete, finite representation of continuous RFVs. The finite number of nodes or elements from which the statistical output moments are computed in a numerical simulation (single realization or Monte Carlo) introduce significant error in the sample statistics (see chapter 8). Therefore, if only a small number of elements will violate the discretization constraints imposed for purely numerical reasons, the statistical results should not be altered significantly. This would allow to weaken the Peclet constraint (6-1) imposed on the grid-design, which is otherwise determined by the largest α value in the random field. Depending on the input parameters, the weakened constraint may allow a considerably larger grid-size than a strict application of (6-1), particularly if α or - for that matter - any pore-size distribution parameter is distributed log-normal, as found in field applications (e.g. Wierenga et al., 1991; White and Sully, 1992).

6.2.2 Block Subdiscretization

Block subdiscretization is a technique applied specifically to nonlinear problems. For the purpose of this study, blocks are defined as the largest homogeneous, discrete units in a random field to distinguish them from the elements in a finite element or finite difference grid. A block is either equivalent to an element or it is subdivided into several elements. The technique of subdividing a (homogeneous) block into several elements is often used for the one-dimensional simulation of infiltration into vertical soil columns consisting of several (random or deterministic) layers of material with different physical properties (e.g. Hern and Melancon, 1986; Yeh and Harvey, 1990). Each layer is modeled by a small stack of cells or elements to accurately capture the non-linear behavior of the matric potential within each layer (Figure 6.1). Examples of using block subdiscretization in a two-dimensional, layered problem are found in Hopmans et al. (1988). Subdiscretization has not been applied to multidimensional heterogeneous fields, where the physical parameters vary in both the horizontal and vertical directions. There, the common modeling rule is not to subdiscretize - in other words: each block

is associated with one element (e.g.: Ababou, 1988; Ünlü et al., 1990; Russo, 1991).

Figure 6.1 shows a typical matric potential distribution in layered media. Layers of coarse material exhibit a small fringe at the bottom, within which the matric potential changes drastically, while the head in layers of fine material changes only gradually. The thickness of the fringe is mainly determined by the slope of the unsaturated hydraulic conductivity function. Assuming Gardner's hydraulic conductivity model (4-8), the slope of the hydraulic conductivity curve is characterized by α (Yeh and Harvey, 1990). The thickness of the fringe Δr is approximately of the order $1/\alpha$ (White and Sully, 1992). Hence, for large α, which is characteristic for coarse textured soils, the fringe is much thinner than for small α, which is characteristic for fine textured soils.

If n elements are chosen to be required within the hypothetical thickness of a fully developed fringe $\Delta r \approx 1/\alpha$, then:

$$\Delta r = n\,\Delta x \approx 1/\alpha \quad \text{thus:} \quad \alpha\Delta x \approx 1/n \qquad \textbf{(6-2)}$$

This simple heuristic criterion is slightly more stringent than the one inferred from the stability analysis by Ababou (1988, p.423; also see (6-1)) and depends on the number n chosen. In applications with correlation lengths much larger than $1/\alpha$ it may be appropriate to discretize heterogeneity on a scale larger than that required for Δx. In those cases a discretization of blocks (which represent the scale of heterogeneity) into several elements may seem justified. However, in the same case random fields can also be generated with a discretization equal to the required element size and several tens of elements per correlation length. No subdiscretization is needed if the typical block-length b (usually 15%-20% of the correlation length) satisfies the condition $\alpha b \approx 1/n$. Numerical examples are used to analyze the effect of subdiscretization.

6.2.3 Correlation Length

Each block in the simulation domain represents a finite, homogeneous portion of the

total domain, within which smaller scale variability is neglected. In geostatistics, these blocks are referred to as "support". Although the term 'support' is closely related to the measurement of certain data (estimation problem), it is here also used as term for the homogeneous blocks in a simulated random field (simulation problem).

In geostatistics it is well-known that the choice of the (measurement) support is crucial to the evaluation of the statistical properties of a RFV e.g., the mean and covariance, because statistical properties are strongly related to the size and shape of the support. Similarly, the size and shape of the simulation support (blocks) has significant impact on the statistical results of the simulation e.g., the mean and covariance of the matric potential h. The simulation should be designed such that the numerical model captures both the spatial variability of K_s and α (input) and the spatial variability of h and **q** (output) with sufficient accuracy. A compromise must be found between representing the natural spatial variability with sufficient accuracy and keeping the computing cost at a minimum.

Geostatistical methods provide simple analytical tools to determine how close the spatial variability of the block values is to the total spatial variability of all the points in a real soil profile. Block values are assumed to be the arithmetic average of all point values within a block. D.G. Krige derived a fundamental relationship that relates the variability of such block values e.g., within a soil profile (the domain of interest), with the variability of all the points within the same soil profile (Journel and Huijbregts, 1978):

$$\sigma^2 (p/d) = \sigma^2 (p/b) + \sigma^2 (b/d) \qquad \textbf{(6-3)}$$

where σ^2 (p/d) is the total variance (of the point values) within the domain, σ^2 (p/b) is the variance of the point values within the block, and σ^2 (b/d) is the variance of the block values within the domain. In applications to subsurface flow problems the arithmetic average, used to derive (6-3), rarely gives an accurate estimate of "effective" values of conductivity on the block scale (Yeh et al., 1985a,b; Gomez-Hernandez, 1991; Desbarats, 1992). The linear geostatistical approach is used here only as an approximation to illustrate the importance of sufficiently resolving heterogeneities. Journel and Huijbregts (1979) applied the variogram to

derive the relationship between 2nd order moments of the point random variable X and the block-averaged random variable X_Ω. In a second order stationary random field, the variogram γ is related to the covariance by:

$$\gamma(\xi) = (\sigma^2 - C(\xi)) \qquad \textbf{(6-4)}$$

A random function that is regularized on the support Ω centered around the point x is defined as:

$$X_\Omega(x) = 1/\Omega \int_\Omega X(y)\, dy \qquad \textbf{(6-5)}$$

The variogram $\gamma_\Omega(b)$ of X_Ω (x) is derived from the variogram $\gamma(p)$ of the point-values by (Journel and Huijbregts (1979, p. 89)):

$$\gamma_\Omega(b) \approx \gamma(p) - \gamma(p,\Omega) \qquad \textbf{(6-6)}$$

Note the similarity of this equation with equation (6-3). $\gamma(p,\Omega)$ is the mean variogram of all points within each block (support) Ω. It is equivalent to the difference between a point variogram (the spatial variability of the point values) and a variogram based on block values (spatial variability of the blocks). $\gamma(p,\Omega)$ is defined by auxiliary functions (see e.g. Journel and Huijbregts, 1979). For rectangular blocks with sides l and L, the auxiliary function is of the following form:

$$\gamma(p,\Omega)=F(L,l)=\frac{2}{L}\int_0^L (L-u)\alpha_\gamma(u;l)du \qquad (6\text{-}7)$$

F(L,l) can be evaluated using charts, numerical solutions, or analytical solutions (Zhang et al., 1990). α_γ is a shape function. Equation (6-7) is used to determine how many blocks per correlation lengths are needed to represent the point variability within a specified error. For example, if the error should not be more than 10%, and assuming an exponential variogram, then $\lambda/b = 15$. A maximum difference between point and block variance of 5% is obtained with a resolution of 30 blocks per correlation length, $\lambda/b = 30$. On the other hand, a resolution of $\lambda/b = 4$ captures only about 70% of the total variance. In such situations considerable error is expected in the estimation of the true variances of the output variables.

Applied to soil water flow, the problem is far more complex than illustrated here, since the above approach (6-7) is based on Bayesian estimation theory, without direct involvement of the physical problem. Also note that point variability is neither a measurable quantity nor a quantity of much interest. It is the upscaling from the field scales of interest to the scales of a simulation that is of importance. The problem of upscaling data based on measurement support to "effective" parameters for the simulation support (blocks) has been discussed elsewhere in the literature (e.g. Rubin and Gomez-Hernandez, 1990). But the simplified analysis given here is helpful to illustrate the principle concern.

6.3 Numerical Simulation

6.3.1 Model Parameters, Initial and Boundary Conditions

Objectives for the numerical simulations here are: (1) model verification: to investigate whether single large field numerical solutions that use a conservative grid-design are comparable to analytical stochastic solutions. (2) grid-design study: to implement a sensitivity analysis by varying several design-related parameters and using field-site related values.

The simulations are based on Gardner's exponential conductivity function (4-8) and the assumption that α is lognormally distributed. In this chapter it is assumed that the RFVs $\log K_s$ and $\log\alpha$ in Gardner's model are perfectly correlated. Then, K_s and α can be derived from a single random field Z by:

$$X = \exp(\mu_X + \sigma_X Z) \qquad \textbf{(6-8)}$$

Z is a N(0,1) normally distributed random process with zero mean, unit variance, and with an exponential covariance structure (2-28) defined by the integral scale λ. The correlation structure is preserved by the transformation such that logX (log: natural logarithm) satisfies the same correlation function as Z. X is the lognormal random process to be derived ($X = K_s, \alpha$). μ_X is the specified mean of the logarithm of the RFV X and σ_X the square root of the variance of the logarithm of X. The mean of $\log K_s$ (where K_s is in [cm/d]) and $\log\alpha$ (α in [1/cm]) are chosen to be 5.5 and -4, respectively. For the model verification the variances for $\log K_s$ and $\log\alpha$ are 0.09 and 0.0009, respectively. For the grid design analysis the variances of $\log K_s$ and $\log\alpha$ are 4 and 0.25, respectively, which is representative of field conditions.

The random fields are generated using the spectral random field generator described in chapter 3. For the purpose of the grid-design sensitivity analysis, which is based on single large random field realizations, differences in the sample input moments from simulation to simulation must be avoided. To achieve a better preservation of the specified moments, the sample mean m_g and the sample standard deviation s_g are computed from the generated random field Z_g. Then the following transformation is applied to obtain Z in (6-8) from Z_g:

$$Z = (Z_g - m_g)/ s_g \qquad \textbf{(6-9)}$$

The numerical solution of Richards equation, given the random field input of $\log K_s$ and $\log\alpha$, is obtained using MMOC2 (chapter 5). All non-variable input parameters to the model are listed in Table 6.1. The parameters are similar to those found for the field conditions at the Las Cruces trench site (Wierenga et al., 1989, 1991). The finite element net in all simulations consists of 200 by 200 quadrilateral elements (rectangles or squares). The boundary conditions are:

a. $q_2 = -10$ [cm/d] at $x_2 = \max$, i.e. constant flux at the top boundary

b. $\Delta h / \Delta x_1 = 0$ at $x_1 = 0$ and $x_1 = \max$, i.e. no flow across the vertical boundaries

c. $\Delta h / \Delta x_2 = 0$ at $x_2 = 0$, i.e. unit hydraulic gradient across the bottom boundary.

x_1 and x_2 are the horizontal and vertical coordinates, respectively, x_2 increasing in upward direction. The steady-state solutions to (4-1 b) are computed by solving the transient solution of an initial value problem (4-1 a) at sufficiently large time. A direct numerical solution of the steady-state Richards equation is not possible due to the heterogeneity of the parameters (see also chapter 7). In addition, near static conditions may develop far from the true steady state (Neuman, 1972).

6.3.2 Model Verification

The model verification consists of a single Monte Carlo realization with a small rectangular element size $\Delta x_1 = 5$ [cm] and $\Delta x_2 = 2$ [cm], a correlation length $\lambda_1 = 50$ [cm], $\lambda_2 = 20$ [cm], and block-size = 1 element. This problem configuration is in conservative agreement with simulations presented by other authors (e.g. Ababou, 1988; Hopmans et al., 1988; Ünlü et al., 1990). To ensure that the perturbations of all RFVs are small, the variances of $\log K_s$ and $\log\alpha$ are 0.09 and 0.0009, respectively.

6.3.3 Grid-Design Analysis

A number of parameters are varied in order to investigate the limits of numerical stochastic models: The element-length $\Delta\mathbf{x}$, the element shape $\Delta x_1/\Delta x_2$, the block-size $\mathbf{b}$, the relative correlation length $\lambda/\mathbf{b}$, and consequently the relative domain size $\mathbf{d}/\lambda$. For the grid-design study the variance of $\log\alpha$ was chosen such that the maximum α does not exceed 0.2 [1/cm]. Strictly applying the grid-Peclet number (6-2) limits the grid-size to less than 10 cm.

In the experiments here the criterion is tested by varying the grid-size from 0.5 cm to 256 cm. The block sizes chosen were 1 element, 2 by 2 elements, and 4 by 4 elements. The (relative) correlation length $\lambda/\mathbf{b}$ varied from the standard 4 and 5 block-lengths to 40 block-lengths. Because the total size of the finite element grid was kept constant (200 by 200 elements), the corresponding domain length varied from 50 λ to only 5 λ. A complete overview of the various simulations is given in Figure 2. Note that up to three simulations are implemented with different grid-size $\Delta\mathbf{x}$ at approximately equal correlation length λ.

Most simulations are implemented with square blocks of 1 and 2 by 2 elements. The simulations with 4 by 4 elements per block are limited to λ = 5 and 10 block-lengths. Rectangular elements are tested for Δ_{x2} = {2 [cm], 4[cm]} with Δ_{x1} = {$2\Delta x_1$, $4\Delta x_1$, $8\Delta x_1$} and $\lambda x_1 = 10\ \Delta x_1$, $\lambda x_2 = 10\ \Delta x_2$,.

All simulations use the same seed for the random field simulator. Simulations based on the same number of blocks but different block-lengths b (i.e. different element-size $\Delta\mathbf{x}$) have an identical random structure. The length-scale of the random structure, however, is different. Simulations based on the same number of blocks but different (relative) correlation length $\lambda/\mathbf{b}$ have similar pattern structures but each with the prescribed correlation length λ. In addition, a Monte Carlo simulation with 30 realizations is implemented with $\Delta x_1 = \Delta x_2 = 4$ [cm], λ = 40 [cm], and block-size = 1 element.

6.4 Results and Discussion

6.4.1 Random Field Generator

The random field generator is known to generate random fields free of numerical artifacts if sufficient discretization of the spectral domain is chosen (see chapter 3). The normalization of the generated random fields (6-9) further decreases the sampling error. The realizations do not contain any obvious artificial structures. None of the random fields exhibit any significant trends and all satisfy the stationarity and normality assumption. The directional sample autocorrelation functions (Yevjevich, 1972) show in more detail the quality of the random fields given various domain sizes for the grid design study (Figure 6.3). The sample correlation functions compare very well with the exponential correlation function, if $D/\lambda \geq 20$ (Figure 6.3c,d). For $D/\lambda \leq 10$ the sample autocorrelation function deviates from the exponential function and shows significantly shorter correlation lengths (Figure 6.3a,b). In this particular realization the horizontal autocorrelation function is less affected by sampling bias than the vertical sample autocorrelation function thus inducing a slight anisotropy. For $D/\lambda = 5$ a significant gap exists between the two curves (Figure 3a). The limitation of the SRFFT based random field generator to large dimensionless domain-sizes ($\lambda' \geq 10$) was discussed in chapter 3.

6.4.2 Comparison with Analytical Solutions (Model Verification)

The simulation runs for the model verification are evaluated with respect to the mean, variance, and covariance, which are compared to analytically derived moments. In chapter 4, the spectral density functions of the head, of the unsaturated hydraulic conductivity, and of the flux components are derived. The mean of the unsaturated hydraulic conductivity and of the flux components are also computed for given constant mean head. In the numerical simulation no head boundaries are specified, only the mean flux is known. An analytical first order

approximation of the mean head is obtained from the relationship for the mean unsaturated hydraulic conductivity (4-35):

$$H = (Y - F) / \Gamma \qquad \textbf{(6-10)}$$

F is the mean of $\log K_s$ and Γ the geometric mean of α. Y is the mean of the unsaturated log conductivity, which can be written in terms of the mean vertical flux (4-43):

$$\exp(Y) = K_m = \langle q_z \rangle \qquad \textbf{(6-11)}$$

For mass continuity the mean vertical flux must be equal to the specified boundary flux (10 [cm/d]) across the top boundary since no flux occurs across the vertical boundaries. With F = 5.5 and Γ = 0.018 [1/cm], the analytical mean pressure head is -174.6 cm, which compares excellently to the mean pressure head of -174.3 cm in the numerical simulation (Table 6.2). The mean values of the other output RFVs are also essentially identical with the first order analytical solution.

The analytical variances are computed from their respective spectral densities by a fast Fourier transform. For the numerical evaluation of the Fourier transforms, spectral density functions are calculated on a 1024^2 grid such that its transform, the covariance function has a resolution of 11 points per correlation length λ_f and a size of 102.4 λ_f in each direction (see chapter 4). The exponential input covariance function is also computed as a FFT of its analytical spectral density function to assess the accuracy of the numerical Fourier transform. The variance obtained for $\log K_s$ through the FFT is 3% below the fully analytical equivalent, which was specified to be 0.09. The accuracy does not improve significantly by increasing the number of points per correlation length or by increasing the size of the FFT domain. Other FFT-analytical solutions from the 1st order perturbation analysis for this verification case are assumed to have a similar margin of accuracy.

Table 6.3 shows that the sample variance of $\log K_s$ (from the random field generator) is within 1% of the specified variance due to the normalization (6-9). The sample variances of logK and the vertical flux are 6% and 14% larger than their analytical variances, respectively. In contrast the head and horizontal flux variances are by 4% and 9% lower, respectively, than

the analytically determined variances. Given the small error of the numerical Fourier transform the remaining 5% to 10% variability in the sample variance must be attributed to sample error. Recall that the 200^2 samples are not mutually independent and the sample size must therefore be considered limited.

The horizontal and vertical sample autocorrelation functions are shown in Figure 6.4 together with the analytically derived autocorrelation functions. The autocorrelation function is obtained from the covariance function by dividing the covariance with its variance. For short separation distances ($\xi' < 2$, where $\xi' = \xi/\lambda_{logK_s}$) the sample correlation of $logK_s$ is in excellent agreement with the analytical exponential correlation function. At larger ξ' the sample correlation in this realization is weaker than expected from the ensemble (analytical) correlation function. This is due to the proportionally smaller sample size from which the correlation is computed as the separation distance increases (Yevjevich, 1972). The smaller sample sizes are associated with larger sampling errors.

A similarly good agreement at shorter separation distances is seen for the correlation functions of the unsaturated hydraulic conductivity logK and the horizontal flux q_h. In contrast, the correlation functions of the head and the vertical flux are significantly different from the ensemble correlation functions even at short lag distances. Since the size and discretization of the FFT domain in the evaluation of the spectral density function is sufficiently accurate, the difference between the ensemble and sample correlation functions must be attributed to sample errors in the simulation. The error of the numerical results is likely due to the limited size of the simulation domain. Both the horizontal and vertical head ensemble correlation functions and the vertical ensemble correlation of v_v have very long correlation lengths relative to the total domain length. The total domain length both vertically and horizontally is 20 λ_f. The vertical and horizontal correlation lengths of the head and the horizontal correlation length of q_v are three to five times larger than for $logK_s$. The domain length is therefore only about six times the correlation length of the head. Since the deterministic flux boundaries increase the variance of the head near the boundary (Rubin and Dagan, 1989) it is not surprising to see a

generally shorter correlation length in the sample correlation functions of the head and the vertical velocity.

Apart from the effects of the limited domain size, the simulations are in excellent agreement with the analytical solutions. The results confirm that the numerical model gives sufficiently accurate solutions under a conservative grid-design. Inaccuracies stem from the limited size of the sample domain given the relatively strong and far-reaching correlation of the head and the vertical velocity.

6.4.3. Grid-Design Sensitivity Analysis

6.4.3.1 Effects on the 1st Moment (Mean)

The analysis focuses on the sensitivity of the head, flux, and unsaturated hydraulic conductivity moments with respect to the various design parameters. Figure 6.5 depicts the sample means of both the input and the output random fields as a function of α_g λ_f. α_g is given as input parameter. λ_f is directly obtained from the random field sample. This is done in an attempt to minimize the impact of varying sample error (6.4.1) occurring due to different relative domain lengths. The correlation length λ of all stochastic variables is computed from the sample covariance functions (Yevjevich, 1972) by iteratively solving the equation:

$$\mathrm{Cov}(\lambda) = \sigma^2 \, e^{-1} \qquad \textbf{(6-12)}$$

This definition of the correlation length λ coincides with the definition of the integral scale if the sample correlation satisfies an exponential correlation function.

The mean values for the input parameters are fairly constant. They show some sample variation due to the different sizes of the random fields generated. Of the output parameters the horizontal mean flux $<q_h>$, the vertical mean flux $<q_v>$, and the mean of the unsaturated hydraulic conductivity <logK> are constant and independent of the grid-size chosen if $\Delta x \leq 16$ cm. The mean head varies significantly depending on the grid-design but also between Monte Carlo runs of the same grid-design. For elements larger than 16^2 [cm^2], all sample mean values

are decreasing. The only exception is $<\log K_s>$, the independent parameter, and $<q_h>$, which always is close to 0. In particular the mean vertical flux $<q_v>$ decreases significantly at large element lengths although it shows very little sample variation at all for smaller elements. Since the flux at the top boundary is specified as 10 [cm/d] and no flux occurs across the vertical boundaries, the decrease in the mean vertical flux rate is an indication of significant numerical mass balance problems. For elements with $\Delta x = 256$ [cm] the decrease in mean vertical flux is more than 20% of the specified flux rate at the top boundary. For the same element size, the mean head decreases by 15 cm or 30% of the observed standard deviation.

The first order approximations of the head disagree even for small element sizes. The first order mean head is 174.6 [cm] (see section 6.4.2), while the numerically obtained mean heads range between 150 and 165 [cm] (based on computations with element lengths of 16 [cm] and less). While the variance of the output RFVs (unsaturated hydraulic conductivity and head) is relatively small, the large variance of the input parameters $\log K_s$ and $\log\alpha$ introduce significant analytical error into the first order approximations of the mean head. This demonstrates the limitations of the first order solutions derived in chapter 4 (see also chapter 8).

6.4.3.2 Variance and Covariance

HEAD: The normalized head variance σ^{*2}_h as a function of α_g and λ_f is computed in a form similar to the one suggested by Yeh (1985b, eqn. 26a):

$$\sigma_h^{*2} = \frac{\sigma_h^2}{\sigma_f^2 \ \lambda_f^2} \qquad \textbf{(6-13)}$$

The normalized head variance for block-size **b'** = 1 (**b=Δx**) is shown in Figure 6.6 together with the analytical function obtained from an evaluation of the first order spectral density of the head. The first order analytical approximation of the 2nd moments of the head and other output parameters are computed assuming a mean head of 155 [cm], which is representative for the mean heads of the numerical computations.

It is assumed that the numerical results for small element size and large λ/b are as accurate in the high input variance case (grid-design analysis) as in the low input variance simulation (model verification, Figure 6.4)). Although there are quantitative differences, the empirical head sample variance follows a stochastic function similar to the analytical variance function. Figure 6.6 shows that for small values of λ_f the first order approximation overestimates the normalized sample variance of the head, while it largely underestimates σ^{*2}_h for large λ_f. For block-size **b'**=1, the choice of the relative correlation length **λ' = λ/b** has a consistent influence on σ^{*2}_h: The larger **λ'** , the lower the normalized head variance. Doubling **λ'** decreases the normalized variance of the head by approximately 10% with the only exception being the case λ/b=40. In other words, the higher resolution of the spatial variability in $\log K_s$ and logα leads to a slightly lower head variance relative to the variance of the independent RFV $\log K_s$. It is interesting to note that unlike the mean head values the normalized head variance does not seem to be significantly altered by large element sizes.

The simulations with block size 2*2el. (**b'**=2**Δx**) and 4*4el. (**b'**=4**Δx**) give results very similar to the single element block simulations (Figure 6.7) regarding the general shape of the empirical variance function. However, here the relative correlation length **λ'** has the opposite effect: The larger the resolution of perturbations (higher **λ'**) the larger the normalized head variance. For 2*2el. blocks the normalized head variance increases by 5% to 10% when doubling the relative correlation length. For 4*4el. blocks, the same increase in relative

correlation length causes a 30% to 40% increase in the normalized head variance. Since a change in relative correlation length changes the number of random points generated (and hence the sample size), it is not clear from these results whether the differences are statistically significant and due to the change in λ' or due to the change in the relative block-size **b'**.

To assess the statistical significance of the results, a small Monte Carlo simulation is implemented with $\mathbf{b'}=\Delta\mathbf{x}$, λ' = (10, 10) to investigate the variability of the sample statistics. Figure 6.7 indicates the range of values in the normalized head variance for 90% of the 30 Monte Carlo samples. The large range of values for the *normalized* head variance is the combined effect of the variability in sample head, in sample correlation length λ_f, and in sample $\log K_s$ variance (see (6-13)). The smallest and largest non-normalized sample head variances differ by a factor of 2. In the Monte Carlo simulation the input λ_f is 40 [cm]. The sample λ_f varies from 34 to 57 [cm]. The sample variance of $\log K_s$, σ^2_f, ranges from 3.6 to 4.5. The range of sample mean head values obtained from each of the Monte Carlo runs is equivalent to approximately 1/2 the head standard deviation. This shows that a single large field simulation can only give rough estimates of the head variance. The range of the sample moments is much larger even than the total range covered by the simulations with different element-, block-, and correlation length. Hence, the differences for the various choices of element size, relative correlation length λ_f', and block size **b'** observed for element-lengths not exceeding 32 cm are statistically of limited significance. For a high level of accuracy, the choice of the relative input correlation length will certainly have to be considered, but then a single large field realization even with 40,000 elements is inadequate. A greater statistical significance can only be achieved by evaluating a large number of Monte Carlo runs and by comparing the results of entire Monte Carlo simulations rather than those of single large realizations. This is beyond the scope of this chapter. However, the results for different element size $\Delta\mathbf{x}$ but identical resolution λ_f' and block-size **b'** are directly comparable, since they are based on the same set of random numbers.

For the (output) correlation length λ_h of the matric suction head the results are similar: In general, $\log\lambda_h$ is linearly proportional to $\log\lambda_f$ (Figure 6.8). For large element sizes (large λ_f)

only insignificant deviations from a log-linear relationship are observed. Like σ_h^2, λ_h shows a dependence on the choice of the relative (input) correlation length λ': As λ' increases from 5 to 40, λ_h decreases, independent of the block-size chosen. Comparing the correlation structure for various block-sizes, it seems that the results are not sensitive to the block-discretization e.g., for $\mathbf{b} = \Delta\mathbf{x}$ and $\lambda = 10\mathbf{b} = 10\Delta\mathbf{x}$ the head correlation is the same as for $\mathbf{b} = 2\Delta\mathbf{x}$ and $\lambda = 5\mathbf{b} = 10\Delta\mathbf{x}$. The exact match is mere coincidence, given that the first simulation was based on a random field of 40,000 numbers, while the latter simulation was based on a random sub-field of only 10,000 numbers.

FLUX: The simulated normalized empirical flux variances $\sigma_{q^*}^2$:

$$\sigma_q^{*2} = \frac{\sigma_q^2}{\sigma_f^2 K_m^2} \qquad \textbf{(6-14)}$$

$$\textit{where:}$$

$$K_m = \exp(F)$$

are approximately 30% to 50% above the theoretical 1st order analytical results if $\alpha_g\lambda_f < 1$. The differences between the numerical and the analytical results increase as $\alpha_g\lambda_f$ increases. The normalized vertical flux variance deviates even qualitatively from the stochastic analytical results at correlation lengths corresponding to element sizes $\Delta x > 16$ cm indicating large numerical errors with discretizations in excess of much more than 16 cm. The increase in vertical flux variance for the larger element sizes coincides with the decrease in the mean vertical flux, further indicating that the vertical flux moments of all output moments are the most sensitive to the element size. The actual (non-normalized) vertical flux variance (like the vertical flux mean) is approximately constant for $\Delta x \leq 16$ cm (Figure 6.9).

The horizontal flux variance follows a similar stochastic form as the analytical solution over the range of all correlation lengths/element sizes. The sensitivity of the flux variances to element-length $\Delta\mathbf{x}$, block-size $\mathbf{b}'$, and relative correlation length λ' is in general slightly smaller than the sensitivity of the head variance to these parameters. Although not explicitly shown

in Figure 6.8, the normalized flux variance of both the vertical and the horizontal flux decreases as the relative correlation length λ' increases. However, the range of variances obtained from different random fields in the Monte Carlo simulation again indicates the weak statistical significance of those results due to the sample error associated with one single large realization when assessing uncertainty of unsaturated flow.

A plot of the vertical and horizontal correlation length λ_{qv} vs. λ_f reveals a very strong correlation to the input correlation length over most of the range tested. Strong deviations from a log-linear type correlation between λ_{qv} and λ_f occur for $\Delta x \geq 64$ cm (Figure 6.10). Figure 6.11 shows the same results for the horizontal flux $\mathbf{q_h}$. Unlike λ_{qv} the numerically determined correlation length of the horizontal flux λ_{qh} slows rather than accelerates its growth relative to λ_f for $\lambda_f > 100$ cm. The analytically derived λ_{qv} and λ_{qh} show a similar nonlinear dependence.

These results for the correlation length of the two flux components as an integrated measure of the covariance function are rather independent of the block-size chosen. The block-size itself has a small influence on the results. Given the range of possible outcomes of the normalized flux variance from a small Monte Carlo simulation, both the influence of the block-size and of the relative correlation length are almost negligible.

UNSATURATED K: A plot of the variance of logK against $\alpha_g\lambda$ and a plot of the correlation length of the unsaturated hydraulic conductivity against the input correlation length of logKs reveals that the unsaturated hydraulic conductivity are little sensitive to the tested grid-design options for $\Delta x \leq 32$ cm (Figure 6.12a-c). As for other statistical output parameters, the variation of sample moments within a single Monte Carlo simulation exceeds the variations observed due to different grid-design. Since the dependence of the logK moments on block size and relative correlation length is much less than the uncertainty arising from the small sample size and hence from the variability in the sample moments there is little further insight these simulations can shed.

As expected, a strong linear dependence exists between λ_y and λ_f. The shape of the unsaturated variance function is similar to the vertical flux variance function. Note that the

vertical flux has a correlation length approximately equal to the input correlation length, while the correlation length of the unsaturated hydraulic conductivity is only about half of λ_f (Figure 6.12b,c). The analytically determined correlation lengths (1st order) are generally larger than the numerical ones. Only at large $\lambda_f > 32$ cm both the horizontal and the vertical correlation length of logK are above the analytical results and also deviate from the linear correlation with λ_f.

6.4.3.3 Rectangular vs. Square Elements

To investigate the numerical effect of the ratio between the horizontal and vertical length of an element, an anisotropic field is simulated once with rectangular blocks consisting of several square elements and once with rectangular blocks consisting of a single rectangular element. Each block consists of only one row of elements in the vertical direction. The block-side ratios b_1/b_2 in the five cases examined are 2, 4, and 8. The relative correlation length λ' is 10 in both the vertical and horizontal directions. Table 6.3 compares several selected results obtained with the square element solutions vs. the rectangular element solutions. For the block-size ratios in these examples there is a remarkable agreement between both types of element shape. The difference in output parameter variance is generally less than 5% of the respective total variance. While the variance of the unsaturated log hydraulic conductivity is slightly smaller for square elements than for rectangular elements, all other variances are slightly larger for square elements than for rectangular elements. The differences in the correlation length are on the order of 1%. The correlation length of the square elements is always slightly smaller than for rectangular elements. Overall no particularly strong bias is found associated with different element shapes.

6.5 Comparison with Other Heterogeneous Flow Simulation Studies

The general framework of the numerical experiments is similar to simulations reported by Hopmans et al. (1989), Ünlü et al.(1990), and Russo (1991). The grid-design analysis not only allows the assessment of the effect of various design parameters but also sheds some valuable insight into the stochastic analysis of flow in heterogeneous porous media. In the following paragraphs the results from section 6.4 are compared with the Monte Carlo simulation results obtained by the above authors.

Russo (1991) and Russo and Dagan (1991) (referred to here as R&D) simulate and evaluate an infiltration event in heterogeneous, unsaturated media in two dimensions with a single large domain simulation. Their computer simulation solves Richards equation with θ, the water content, instead of the matric potential h as dependent variable. The input RFVs are generated based on the similar media theory (Warrick et al., 1977), which requires one random field from which all random input variables are derived (compare to (6-8)). Unlike the simulations here, their simulation was based on VanGenuchten's constitutive equations for $K(\theta)$ and $\psi(\theta)$. Their grid-discretization was within the framework tested here (Δx=20 cm, Δz=2 cm). The simulation was based on a grid with just over 30,000 nodes with a relative domain size $\mathbf{d'}$ =(15, 80) in the horizontal and vertical direction, respectively. Since the resulting correlation length of the water content is similar to the input correlation of the scaling factor, the simulation results of the water content moments have less sampling error than the head moments in the simulations implemented here. But no attempt is made to characterize the sample variance of either the input or the output stochastic sample parameters.

In their analysis R&D suggest that

$$(\sigma^2 \lambda)_y = (\sigma^2 \lambda)_f \qquad \textbf{(6-15)}$$

reasoning that under unsaturated conditions the correlation length of the conductivity decreases and the variance increases. Clearly, the simulations here demonstrate that the relationship does not necessarily hold. R&D concluded that the unsaturated hydraulic conductivity variance increases reciprocal to the decrease in correlation length as the soil dries out. However, the behavior of σ^2_y among others depends primarily on the set of unsaturated hydraulic conductivity

functions generated and on the mean hydraulic head in the simulation. This is true for both Gardner's and VanGenuchten's expression of K(h) and will be determined by the mean and variance chosen for the parameters in the K(h) expression. Field evidence qualitatively supports these findings (White and Sully, 1992). In the simulations described above σ^2_y is smaller than the variance for the saturated hydraulic conductivity σ^2_f: The correlation of f and logα causes a continuous decrease of the unsaturated conductivity variance as the mean head decreases until it reaches a minimum near $h_{min} = -1/(\alpha_g \zeta)$ (see Figure 6.13). At heads drier than h_{min} the unsaturated conductivity variance increases with decreasing head. While the reduction of σ^2_y is an artifact of the selected model, it should be understood that parameters are generally chosen to fit measured data with the K(h) function. In particular, if Gardner's exponential expression is chosen, the parameter $\log K_s$ should not be mistaken for the actual saturated hydraulic conductivity. Gardner's function is known to work well only for a limited range of suction values. If a wide range of h is expected to occur during the simulations, VanGenuchten's or other K(h) relations may be more satisfying. In general, however, a statement like (6-15) is not warranted given the strong dependence of σ^2_y on the K(h) function.

As a consequence of the hypothesis (6-15), R&D also discuss the possibility that unsaturated transport variability may be governed by similar laws as saturated transport due to the fact that the "*Lagrangian analysis [...] is of general nature and applies to saturated and unsaturated flow as well.*" In particular they find for their simulation, that

$$\sigma_{qv}{}^2/\langle q_v \rangle^2 \, \lambda_{qv} = \sigma^2_f \, \lambda_f \qquad \textbf{(6-16)}$$

The results in section 6.4 partially supports their conclusion. Indeed remarkably close agreement with (6-16) is found if the variance and correlation length of $f=\log K_s$ is replaced with the variance and correlation length of $y=\log K$ (Figure 6.14). However, (6-16) does not hold for $\log K_s$ as suggested by R&D. This precludes an *a priori* determination of the longitudinal dispersivity from σ^2_f and λ_f alone. A linear regression curve through the experimental values also exhibits a slope slightly larger than 1, which does not seem to be caused by the larger $\Delta\mathbf{x}$ alone (see the case, where $\mathbf{b} = 1\Delta\mathbf{x}$).

A further hypothesis tested by R&D suggests that according to theoretical results suggested originally for saturated flow, the unsaturated flux moments are characterized approximately by:

$$CV_{qz}^2 = \sigma_{qv}^2/\langle q_z\rangle^2 = 0.375\ \sigma^2_f \qquad \textbf{(6-17)}$$

In neither Russo's nor the simulations in 6.4 does this particular relationship hold. But if σ^2_{logKs} is again replaced with σ^2_{logK} the agreement between the numerical results and (6-21) is quite good: In the simulations of section 6.4 $CV_{qz}^2/\sigma^2_{logK}$ varies from 0.24 to 0.31 for the simulations with single element blocks, from 0.25 to 0.40 for 2*2 element-blocks, and from 0.28 to 0.34 for the 4*4 element blocks. This supports the hypothesis that the stochastic theory developed for the saturated velocity field may hold for the unsaturated field, with logK replacing logKs (Figure 6.15) (see also chapter 9).

The results presented here are also in agreement with some of the findings of Hopmans et al. (1988) (referred to here as Hopmans), who simulated 2-D infiltration into one- and two-layered soils. In their simulations of the one-layered case, the simulated soil consists of a set of random soil property block-columns, each of which is subdivided into homogeneous (finite difference) elements. They find that the head values converged quickly to the ensemble moments. Only 10 Monte Carlo simulations with 50 random soil columns (approximately corresponding to a single realization with 500 random soil columns) were needed to achieve convergence, a result that is in clear contrast with the findings of section 6.4. As shown previously even a single realization of 40,000 random blocks may not be considered to give results of the accuracy reported by Hopmans. The reason for the apparent discrepancy between Hopmans results and those reported here are the following: (1.) The bottom boundary condition in Hopmans simulation is fixed with respect to the head, thereby greatly reducing the head variance in most of the simulation domain. (2.) Hopmans' random fields are random only in the horizontal direction. The variance in Hopmans simulation varies between 80 and 400 cm^2 compared to a range from less than 5 cm^2 to more than 1000 cm^2 in the simulations presented here. In contrast to the strong horizontal head correlation of the simulations in this study, the

correlation length in Hopmans' simulation was only slightly larger than the input correlation length and did not exceed 3 Δx or 1/15 of the domain size in the horizontal direction (Hopmans et al, 1988, Figure 5).

Hopmans used correlation lengths (in the definition of (6-12)) of 2 blocks and 4 blocks. Like in the simulations of this study, a small but discernable difference was found in the head correlation length that might be attributed to the better resolution of the heterogeneous properties: Their table 5 also indicates a slight decrease in the correlation length of the head as the relative input correlation length increases.

The results in 6.4 regarding the stability of the mean head and flux confirm similar findings of Ünlü et al. (1990) (here referred to as Ünlü). Their one-dimensional, vertical, transient flow simulations showed a similar behavior of the head and flux variance as a function of the input variance as Hopmans simulations and the simulations ins section 6.4. Furthermore, the simulations in this study confirm the conclusion of Ünlü, that the flux variance in mean flow direction increases, if the correlation length in mean flow direction increases, while the vertical flux variance decreases, if the correlation length in the horizontal direction increases: In the simulations with varying element-width Δx_2, but element-"thickness" Δx_1 (and consequently a change of λ_{x2} but not of λ_{x1}) the simulations with larger λ_{x2} have a significantly smaller variance in q_{x1}, while the variance of q_{x2} increases. In all other simulations, the simultaneous change in width and thickness of the element (to keep the square form) and hence in λ caused a decrease in σ^2_{qh}, but an increase in σ^2_{qv} for any constant $\lambda/\mathbf{b}$ and $b/\Delta x_1$. Although discernable, the increase in the vertical flux variance is by far not as drastic as observed in the 1-dimensional simulations of Ünlü. This is expected due to the higher degree of freedom in the flow-path for the 2-D simulations (see also Yeh, 1985a).

6.6 Conclusion and Summary

The previous analysis of several dozen flow simulations with varying element-size,

block-size, and correlation-length allows valuable insight into the accuracy of numerical stochastic solutions and its dependence on grid-design. The simulation further sheds some light on previous analyses by various authors.

As part of the model verification the numerical solutions for the stochastic moments of the head and flux (mean, variance, and covariance) are found to compare well with the analytical results for 2-D flow that were derived in chapter 4. The only disagreement found between analytical and numerical results are the covariance functions of the head and the vertical flux. Both the head and the vertical flux have very long correlation lengths, several times longer than the input correlation length λ_f. The size of the domain (200 by 200 elements or 20 by 20 correlation lengths) is found to be inadequate to unbiasedly sample the head and vertical flux. As a result the numerical covariance functions are of significantly shorter correlation length than the analytical covariances for the head and the vertical velocity.

The grid design sensitivity analysis was implemented with parameters chosen to be representative of field conditions. The conservative grid-design simulation results served as comparative basis for the sensitivity analysis. Since the input parameters have a large variance, the analytical solutions derived in chapter 4 cannot serve as a direct verification tool for the grid design sensitivity analysis. Instead it may serve as a guideline only. Indeed, the moments of the numerical simulation significantly differ from the analytically determined moments, even for the same conservatively chosen grid-design. But the general qualitative dependency between stochastic input and output parameters was found to be similar.

The element-size was found to have little influence on the head solution accuracy as long as 32 cm thickness and width was not exceeded. Numerical oscillations significantly distort the head and unsaturated hydraulic conductivity moments only if simulations are based on element-sizes of 64 cm and larger. The vertical flux moments are more sensitive to the grid-design than the head moments and require an element size of 16 cm or less in the vertical direction. A grid-Peclet number $\alpha\Delta x < 2$, derived for the quasi-linear form of Richards equation, gives a very safe margin if it is strictly applied such that the condition is met for all

elements. Based on the findings of section 6.4 a weaker grid-Peclet number restriction can be formulated:

$$\alpha_g \Delta x < 0.5 \qquad \textbf{(6-18)}$$

where α_g is the geometric mean of α. This criterion is simple to implement, gives larger freedom in the choice of the element-size and still provides accurate solutions. For most practical purposes, this allows grid-sizes of up to 20 cm and more in the vertical direction. The element size in the horizontal direction is by far not as critical, and horizontal element lengths of e.g. 4 cm and 32 cm give identical results.

The subdiscretization into multi-element blocks for better resolution of the nonlinear head variations gave little improvement in the accuracy of the solutions. The differences to the simulations with single-element blocks were subtle and statistically of little significance. If $b=\Delta x$ is sufficiently small to give a good resolution of the heterogeneities (i.e. $b/\lambda \leq 0.1$), and if Δx satisfies the grid-Peclet criterion to avoid oscillations, the error introduced by linear head interpolation between element nodes is reduced sufficiently to be neglected.

The simulations have shown that the choice of a larger relative correlation length has a discernable albeit small effect on the head and flux variance and covariance: With large λ/b the stronger coherence of random input parameters reduces the discrete jumps in hydraulic properties between neighboring blocks. Hence, the nonlinearity in the matric potential field decreases, while its numerical approximation improves. As a result the output variance of the head tends to increase due to a higher resolution of the perturbations and the output head correlation length decreases. In contrast, the flux variance decreases as the perturbation resolution increases. The differences have a weak statistical significance but are in accordance with findings by Hopmans et al. (1988).

By comparing several single large realizations it was found that simulations, which are based on a singe large realization, give stochastic results that are associated with considerable sampling error. Although only results for a limited number of Monte Carlo realizations are available, the variations of the sample correlation lengths and sample variances of head and flux

indicate that a single realization with 10^4 - 10^5 elements and a side-length of 20 λ_f does give results with a sampling error of up to a factor 2.

With respect to previously implemented research, the simulations confirm the hypothesis by Russo and Dagan (1991), that the unsaturated velocity field may be subject to the same stochastic processes formulated for the saturated case. By consistently replacing the moments of logKs with the moments of logK, it was shown that the Lagrangian unsaturated flux moments presented in Russo and Dagan (1991) are related to the unsaturated hydraulic conductivity moments in a manner very similar to that found under saturated condition. The simulations in this chapter are not considered a complete proof of their hypothesis because other factors, like the infiltration rate and the geometric mean of α, may strongly influence the results as well. Here these parameters were kept constant. It would be particularly interesting to investigate the proposed relationships for water movement in dry soils. Most importantly, however, it is also shown that their assumption (6-15) does not generally hold. In contrast to the suggestion by Russo and Dagan (1991), it is therefore not possible to derive the moments of the flux field directly from the moments of the input random field of logKs.

Further research is certainly necessary to obtain a better understanding of numerical grid-design in stochastic simulations of unsaturated flow. This research has not addressed the impact of the infiltration rate on grid-design or the effect of different constitutive functions and constitutive parameters. The soil flow simulations only addressed accuracy for steady-state conditions in a relatively moist soil. The results underline the necessity of a careful grid-design evaluation to avoid numerical errors but also indicate that much more rigorous Monte Carlo simulations are necessary to accurately assess the impact of grid-design. At computation times exceeding 6 to 10 hours even on a dedicated workstation such Monte Carlo simulations are very limited in the number of realizations. The next chapter will introduce a numerical technique that accelerates the numerical computation time by up to two orders of magnitude. With such improvements in the computational techniques, Monte Carlo simulations can easily be implemented with hundreds of realizations. Chapter 8 will present the analysis of unsaturated

flow with multiple realization Monte Carlo simulations.

Table 6.1: Non-variable input parameters common to all simulations of the model verification and grid design analysis.

input parameter	model verification	grid design analysis
mean $\log K_s$	5.5	5.5
variance $\log K_s$	0.09	4.0
mean $\log\alpha$	-4.0	-4.0
variance $\log\alpha$	0.0009	0.25
saturated water content	0.3	0.3
residual water content	0.3	0.3

Table 6.2: Comparison of the sample mean; obtained from a single large scale simulation with the analytical moments obtained from the 1st order perturbation analysis (chapter 4).

MEAN	analytical-1st order	simulation
logKs	5.500	5.513
logK	2.303	2.313
head [cm]	-174.6	-174.3
hor. flux [cm]	0.000	-0.02264
ver. flux [cm]	-10.00	-9.999
VARIANCE		
logKs	0.08742 (0.09)	0.09148
logK	0.03488	0.03694
head [cm^2]	16.59	15.92
hor. flux [$(cm/d)^2$]	0.3828	0.3471
vert. flux [$(cm/d)^2$]	0.5907	0.6708

Table 6.3: Comparison of the sample variance and correlation length for rectangular elements (1st row) and square elements (2nd row). Each column represents a different block-size indicated in the top row. All units are based on [cm] and [days].

rectang./square	4 x 2 cm^2	8 x 2 cm^2	16 x 2 cm^2	8 x 4 cm^2	16 x 4 cm^2	32 x 4 cm^2
σ^2 logK	0.440	0.410	0.388	0.387	0.353	0.339
	0.439	0.406	0.385	0.385	0.350	0.338
σ^2 head	35.9	61.1	103	78.1	134	22.2
	36.4	54.6	104	78.5	128	223.1
σ^2 qh	5.20	4.85	4.07	4.61	3.95	3.08
	5.38	5.12	4.46	4.78	4.19	3.39
σ^2 qv	8.85	6.22	3.74	8.16	5.28	2.72
	8.85	6.73	4.12	8.17	5.74	3.07
λ logKs	31.8	63.6	127.2	63.6	127.2	254
	31.8	63.6	127.2	63.6	127.2	254
λ logK	14.7	28.6	57.1	27.2	532.6	110
	14.7	28.5	57.3	27.2	523.9	111
λ head	68.0	75.8	106	83.1	114.4	183
	68.7	66.3	105	83.3	111.3	181
λ qh	14.3	23.1	37.9	26.7	42.7	73.0
	14.1	23.+	37.2	26.4	42.5	71.5
λ qv	10.0	17.4	27.1	19.0	31.3	48.8
	10.2	17.8	26.1	19.3	31.9	45.4

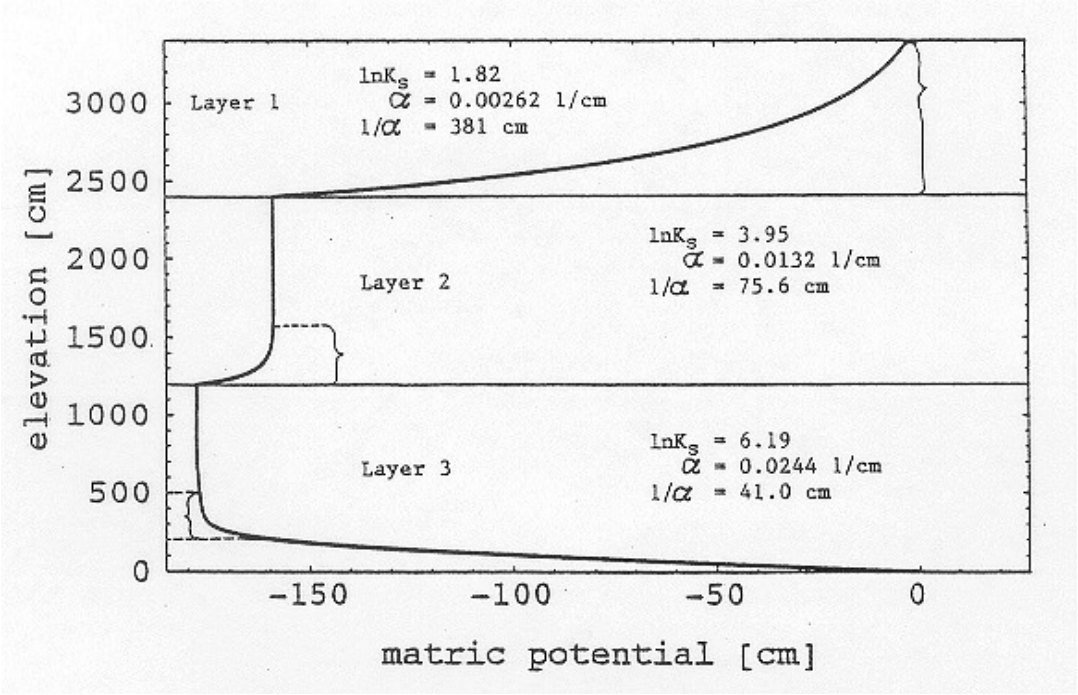

Figure 6.1: Matric potential distribution in a 3-layered soil column. Layer 1 is a very low permeable soil with small α. Permeability and α.increase with each of the subsequent two-layers. Inversely, the nonlinear portion of the capillary fringe decreases. Layer 3 requires smaller discretization than layer 2 or layer 1 to accurately capture the nonlinear portion of the matric potential curve.

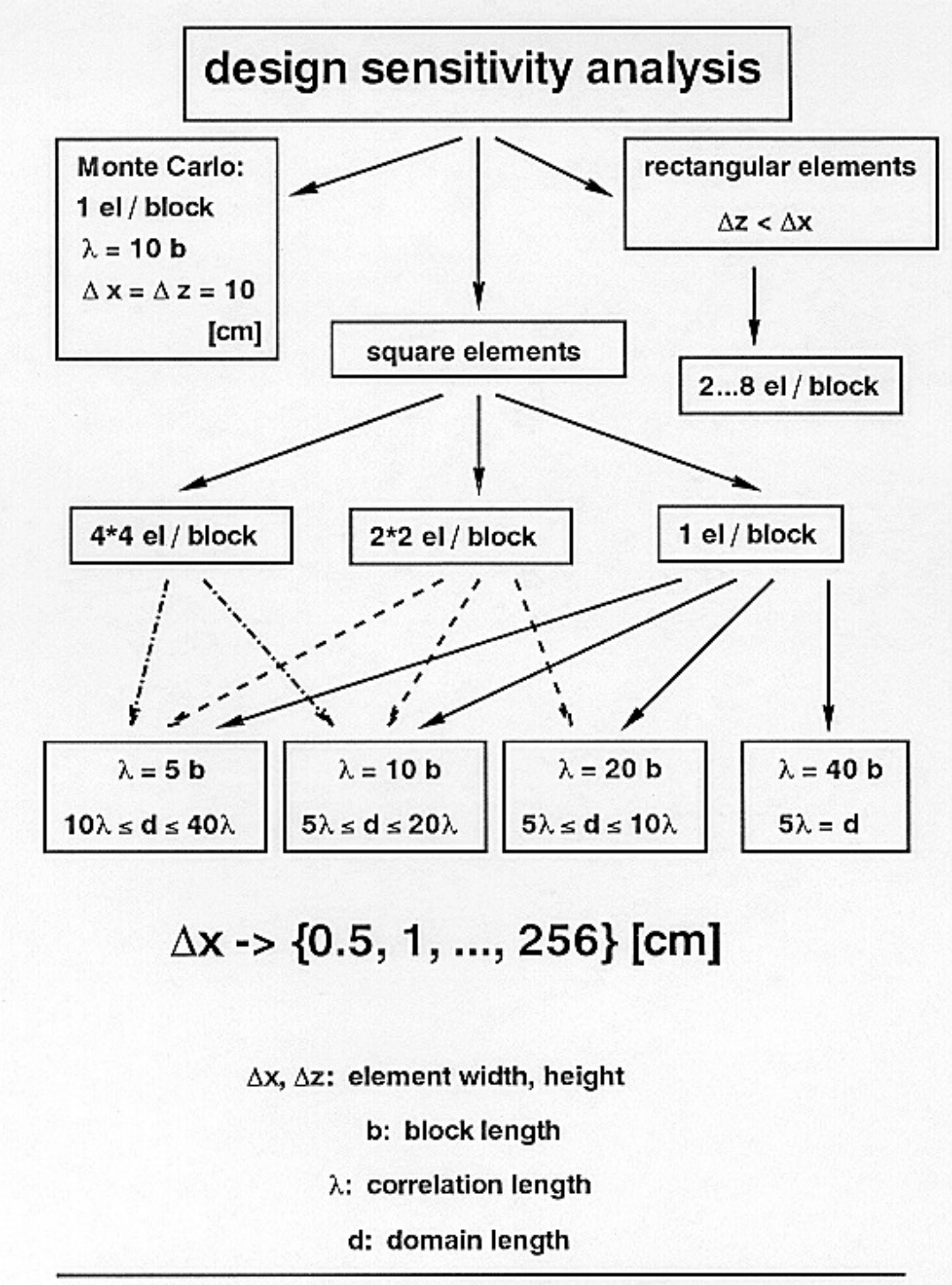

Figure 6.2: Overview of the simulation concept for the grid design sensitivity analysis.

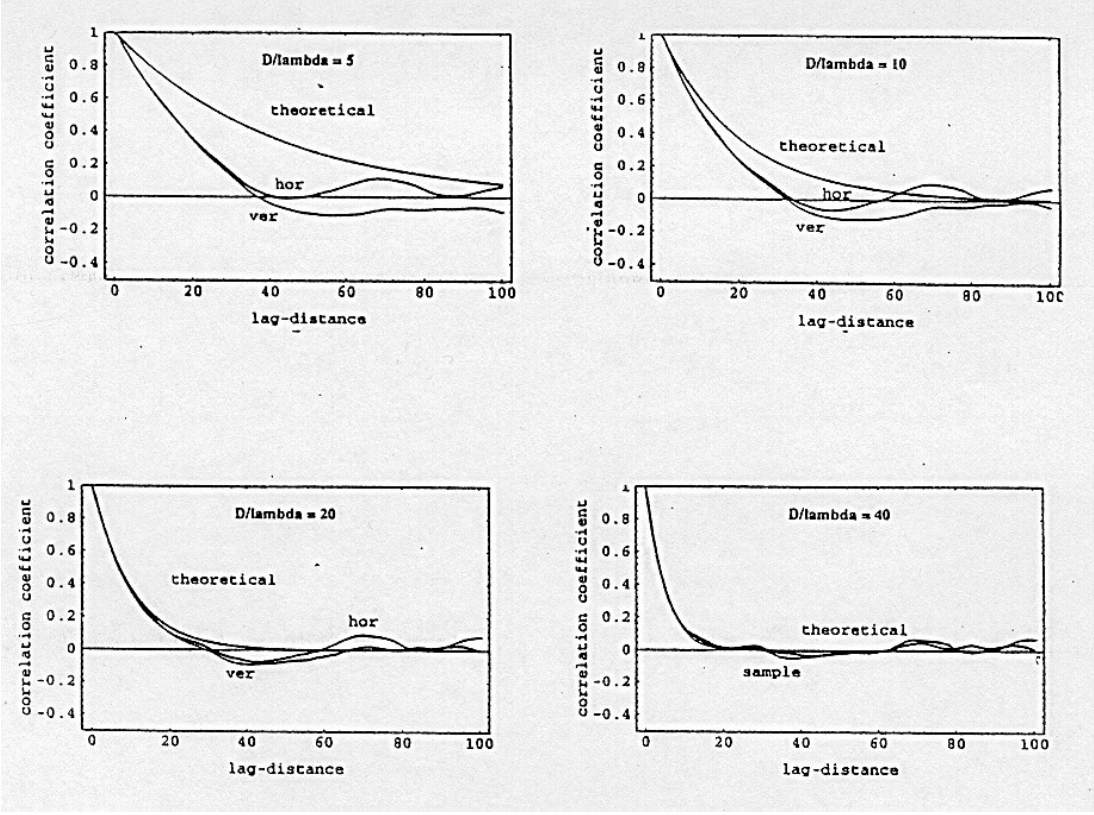

Figure 6.3: Two-point autocorrelation function of the random field for various relative domain sized D/λ. The absolute domain size is 200 by 200 grid points. The autocorrelation function is computed by spatial averaging for lag-distances up to half the length of the random field.

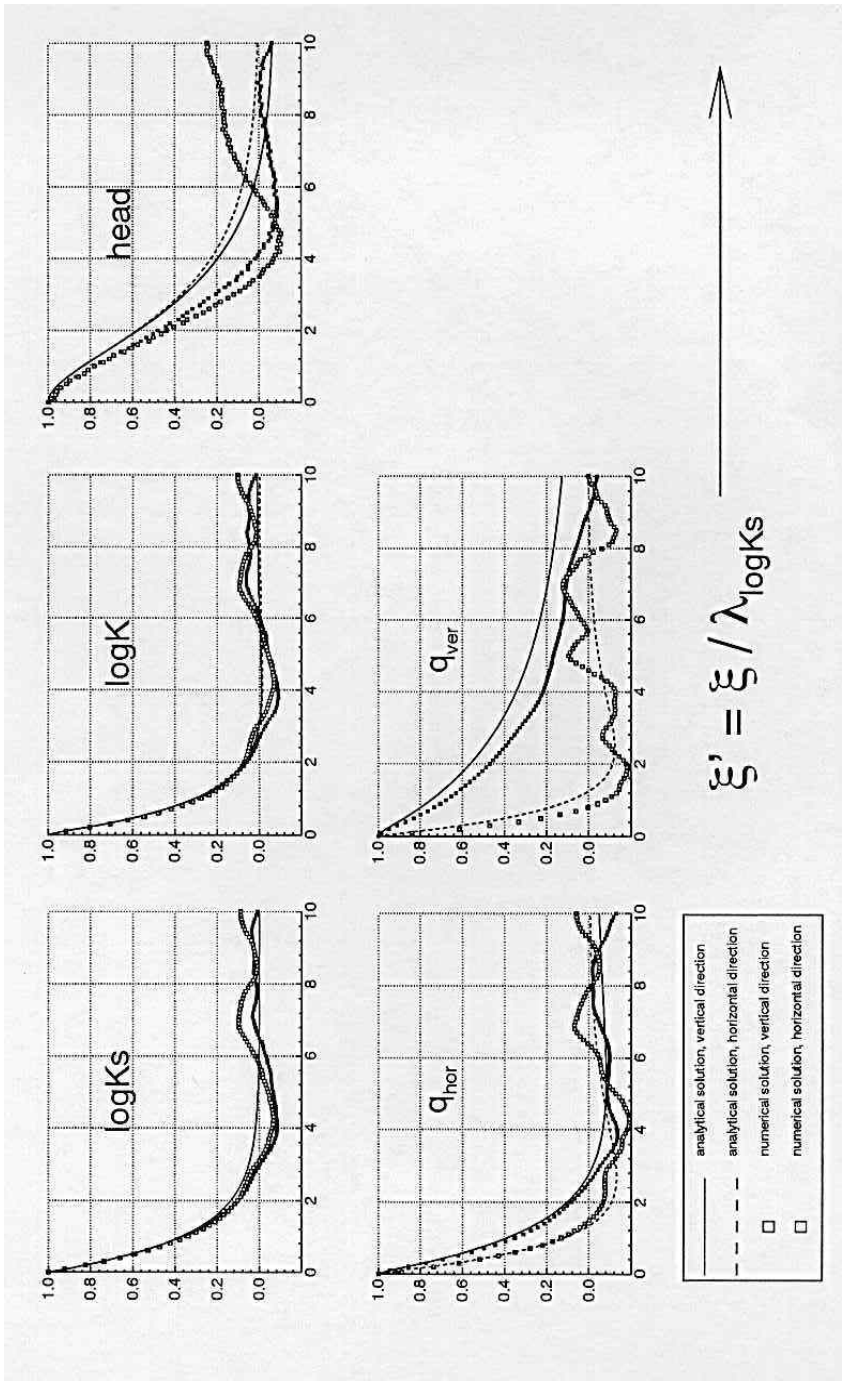

Figure 6.4: and output RFVs.

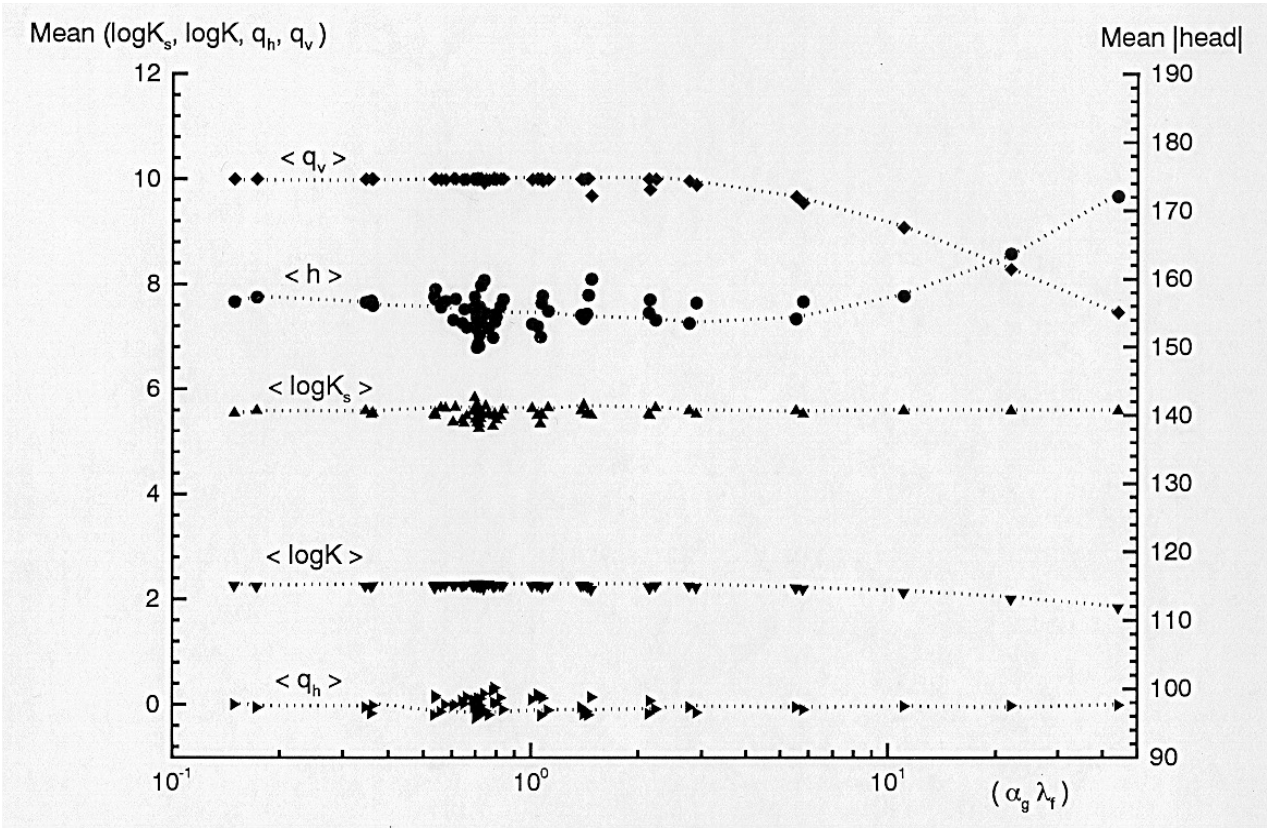

Figure 6.5:

logK

s given

α

g = 0.018 [cm

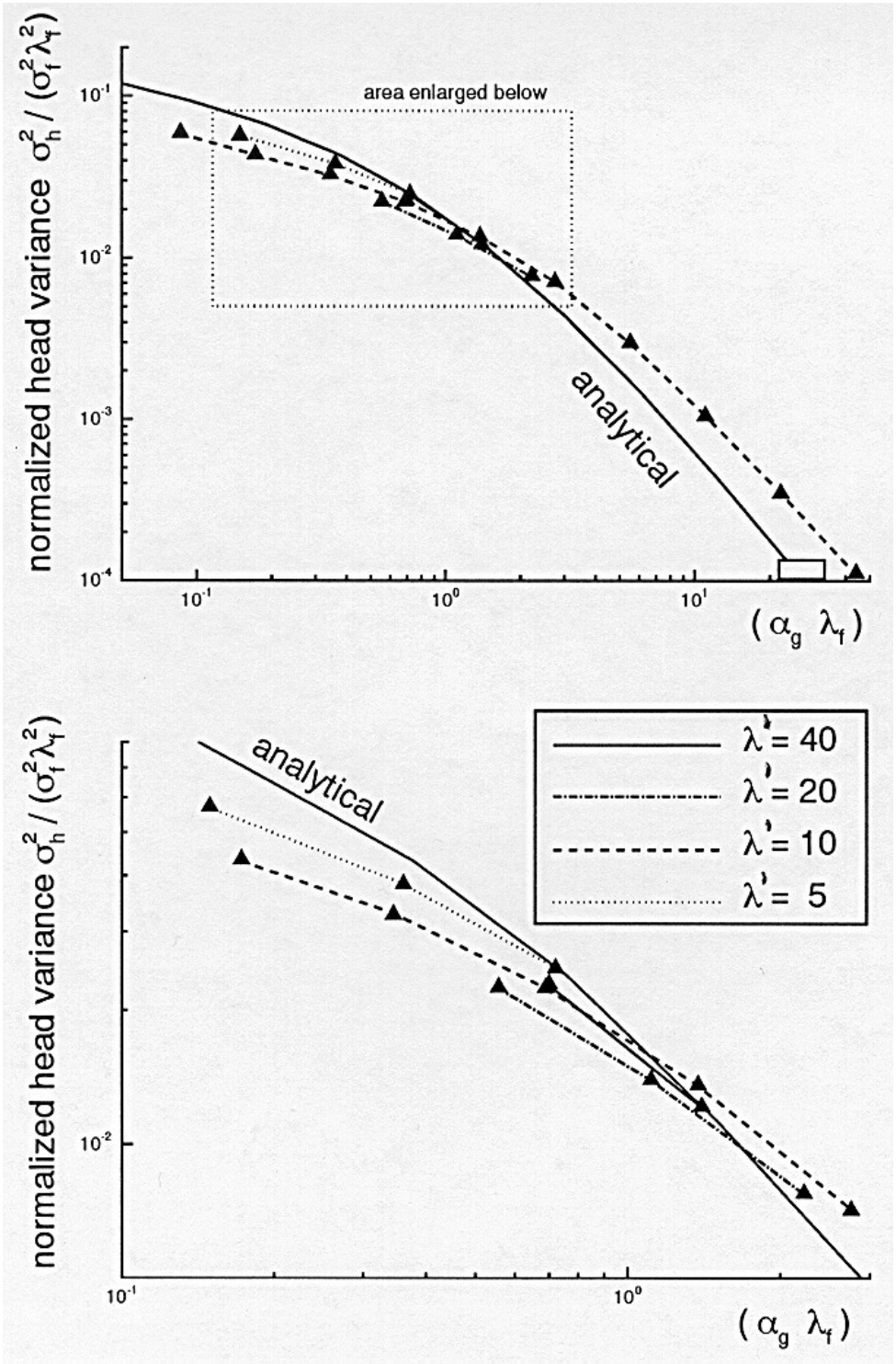

Figure 6.6: Normalized head variance as a function of $\alpha_g \lambda_f$, where λ_f is the sample correlation length of $f = \log K_s$. Only simulations with block-size $b=\Delta x$ are shown.

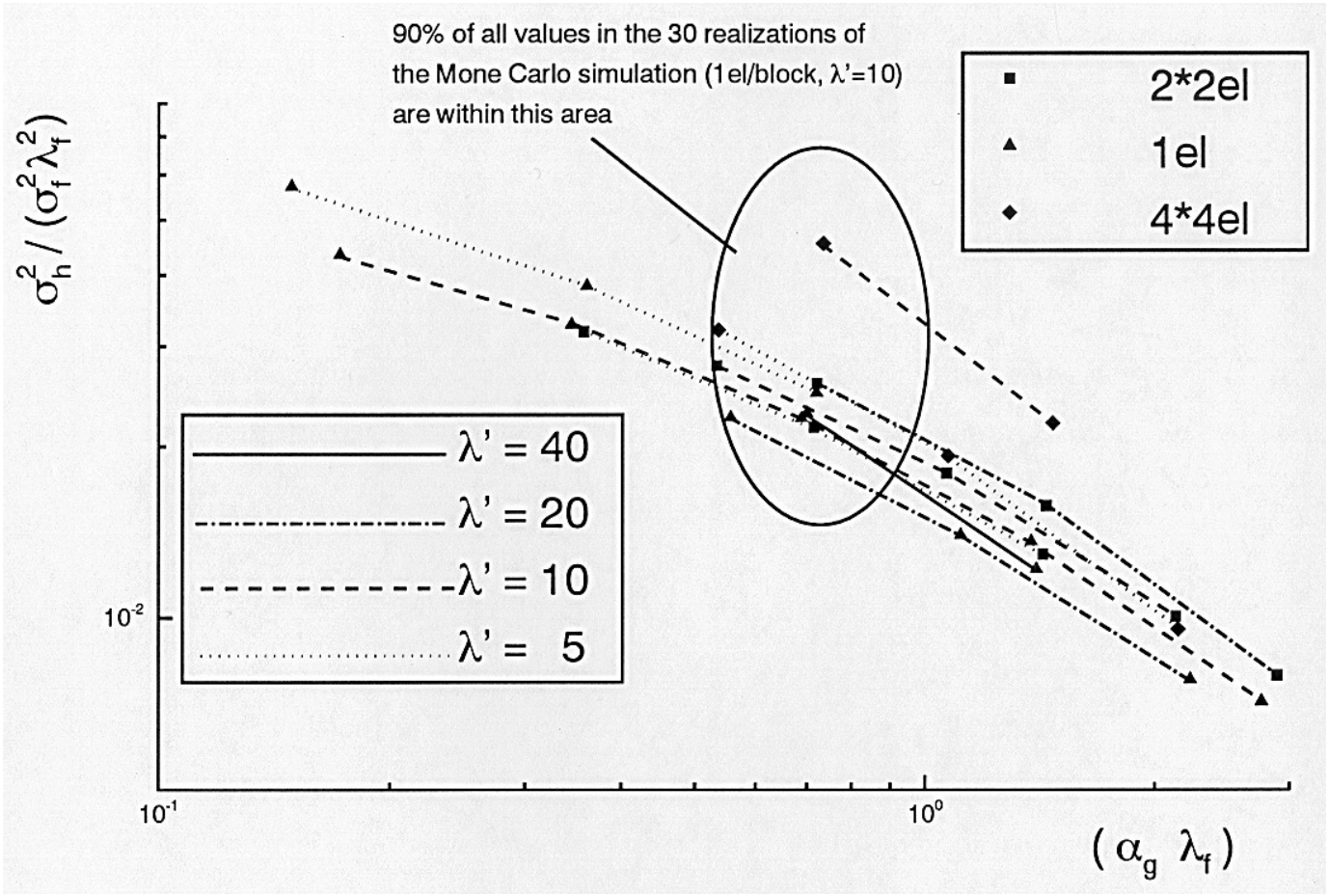

Figure 6.7:

element/block), b=2

$\overset{\Delta}{x}$ (2*2 elements/block), b=4

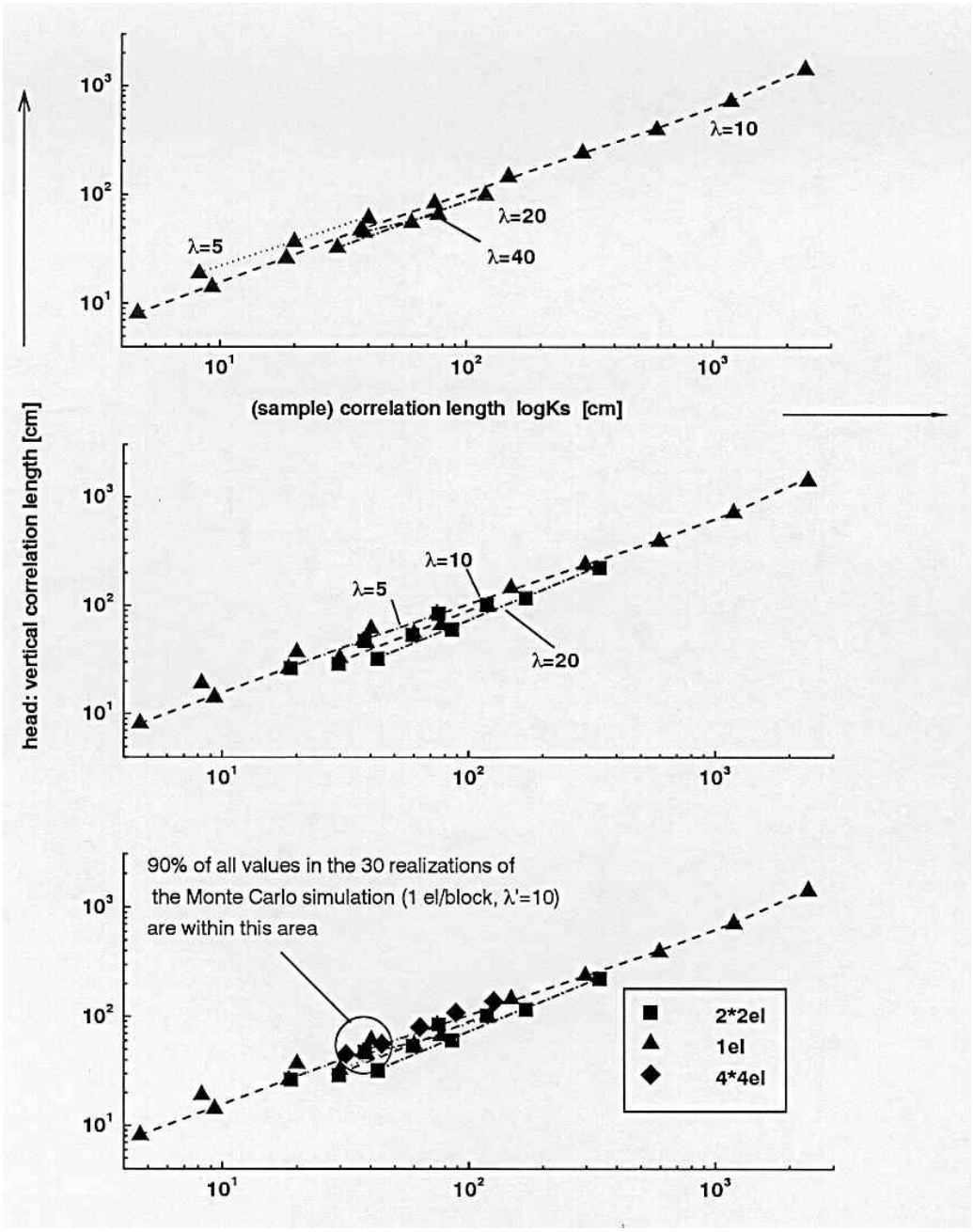

Figure 6.8: Vertical correlation length of the sample head values for each simulation.

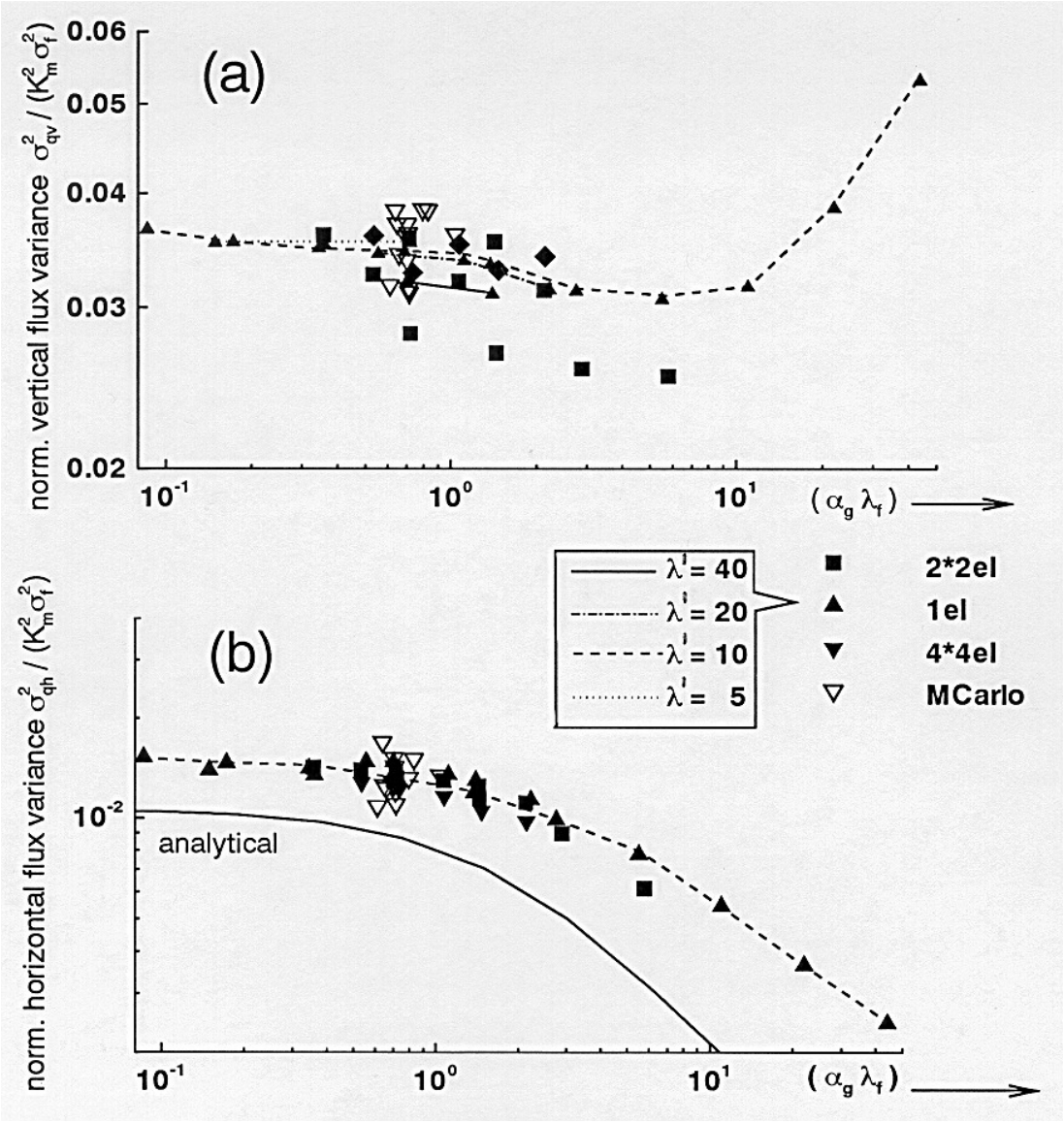

Figure 6.9: Normalized variances of the vertical (a) and horizontal (b) flux. Results from all simulations and from 7 of the 30 Monte Carlo realizations are plotted. The straight line below the numerical data is a first order perturbation solution.

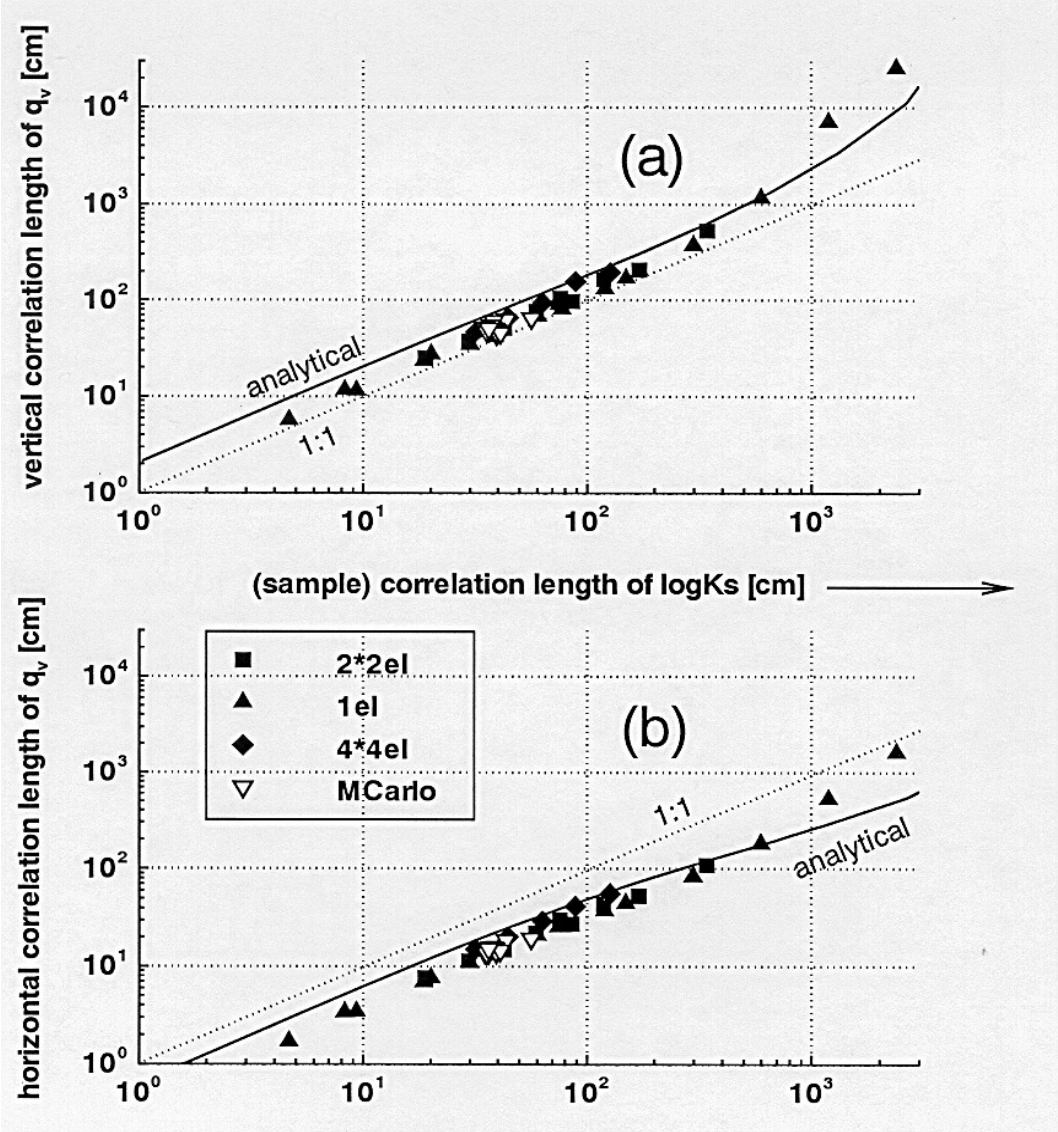

Figure 6.10: Vertical (top) and horizontal (bottom) sample correlation length of the vertical velocity. The solid line is obtained from the first-order perturbation analysis.

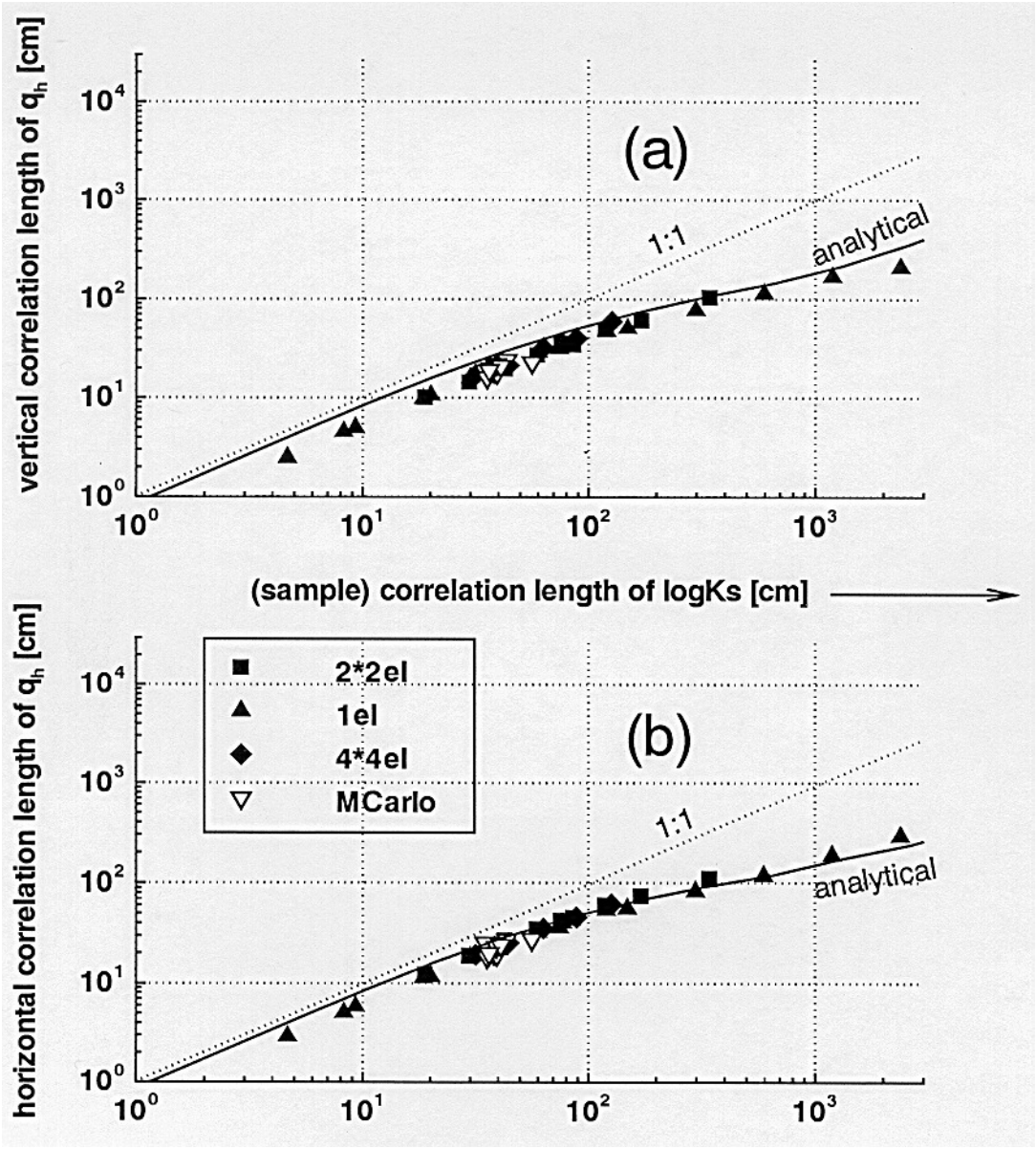

Figure 6.11: Vertical (a) and horizontal (b) sample correlation length of the horizontal velocity. The solid line indicates the first order perturbation solution.

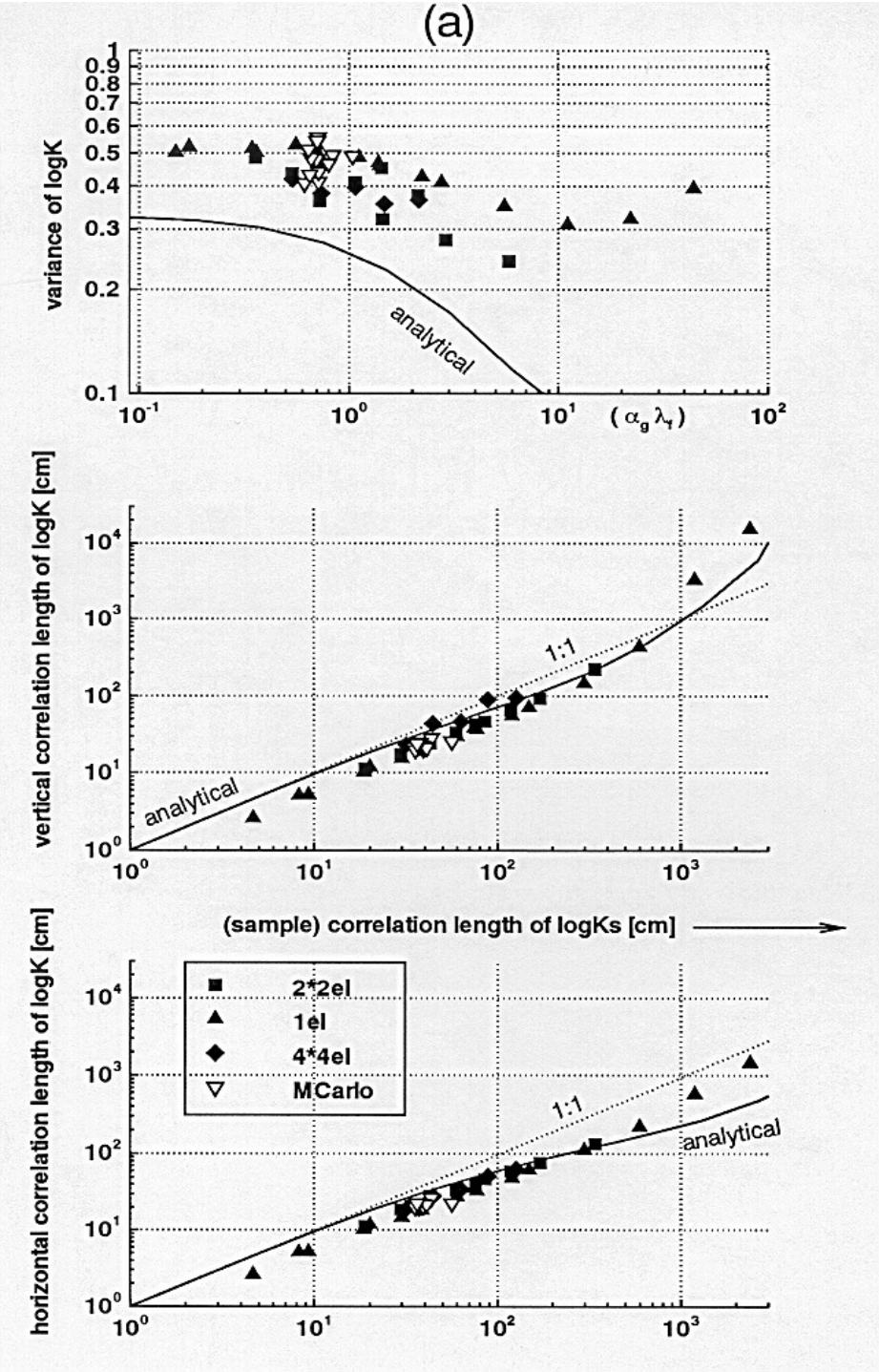

Figure 6.12: Variance (a), vertical (b) and horizontal (c) sample correlation length of the unsaturated hydraulic conductivity y = log K. The solid lines represent the first-order perturbation solutions derived in chapter 4.

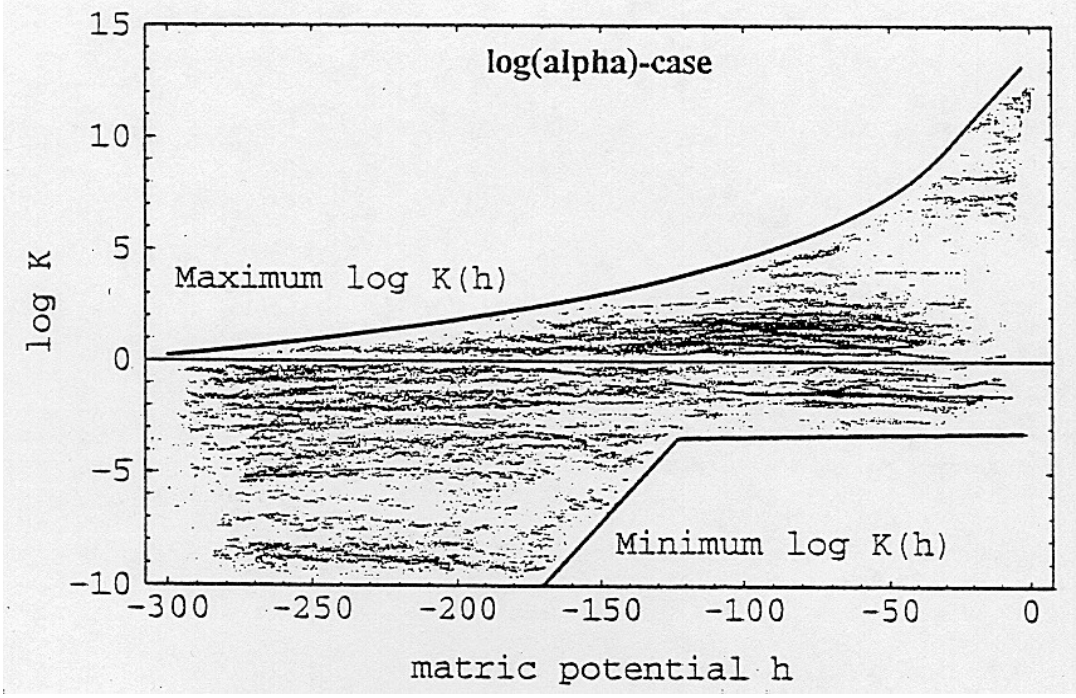

Figure 6.13: Envelope of all possible unsaturated hydraulic conductivity curves in run 1 of the logα-case Monte Carlo simulation.

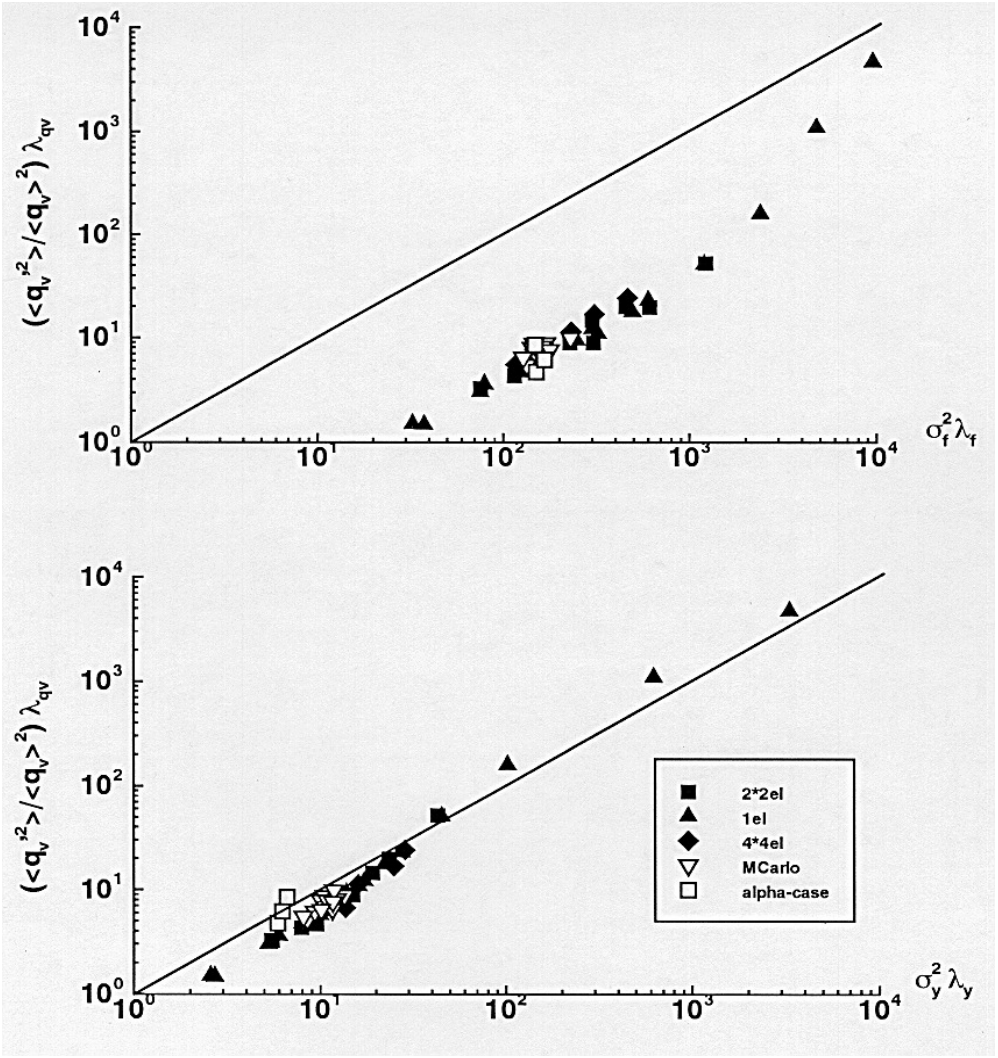

Figure 6.14: The Lagrangian flux field equation (6-16) using sample parameters of the saturated hydraulic conductivity (top) and of the unsaturated hydraulic conductivity (bottom).

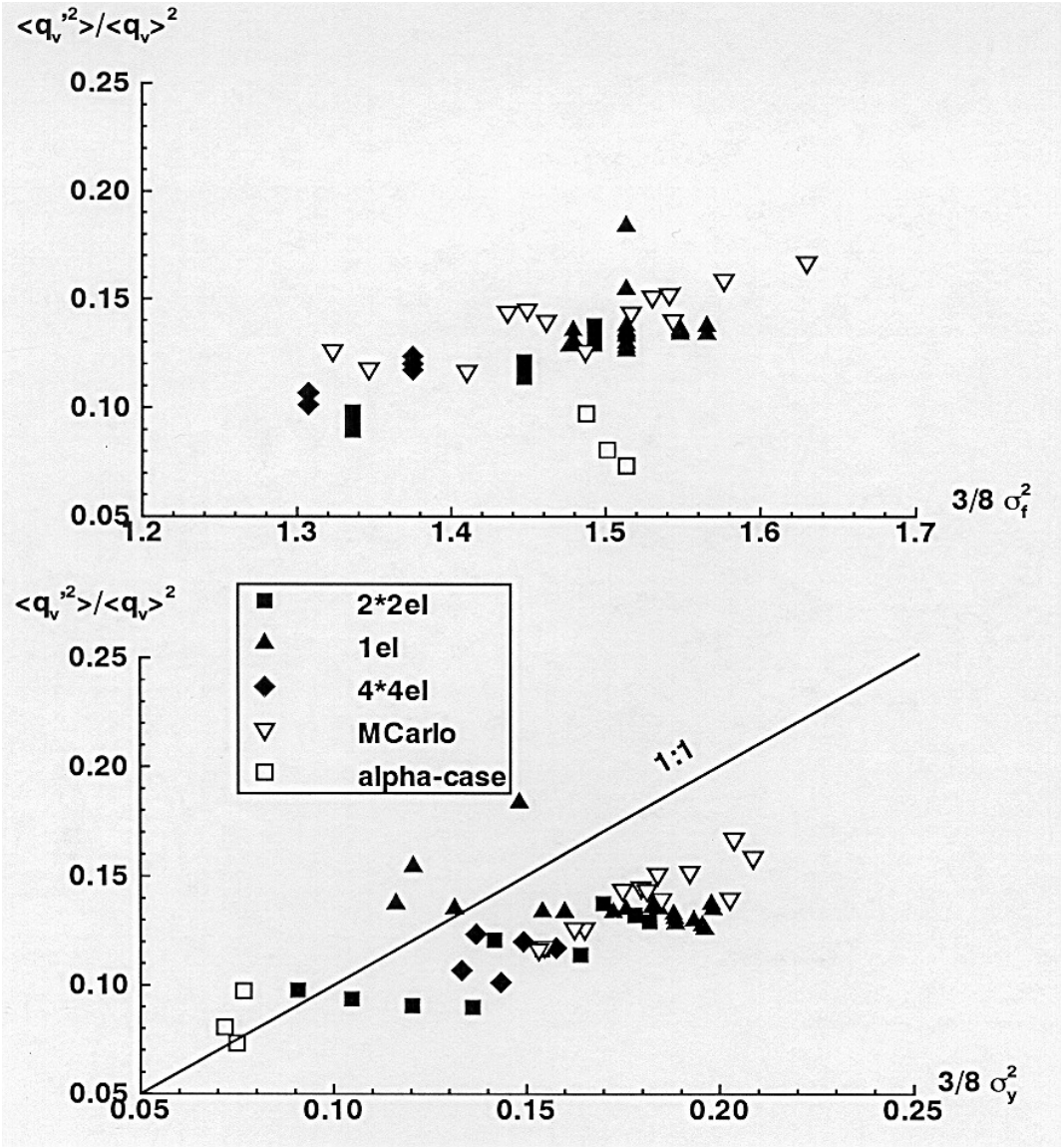

Figure 6.15: Squared coefficient of variation of the vertical flux compared to 3/8 σ_f^2 (top) and to 3/8 σ_y^2 (bottom); see equation 6-17.